Nonlinear Cochlear Signal Processing

Jont B. Allen
Florham Park, NJ

July 19, 2001

Contents

Introduction

This chapter describes the mechanical function of the cochlea, or inner ear, the organ that converts signals from acoustical to neural. Many cochlear hearing disorders are still not well understood. If systematic progress is to be made in improved diagnostics and treatment of these disorders, a clear understanding of basic principles is essential. Models of the cochlea are useful because they succinctly describe auditory perception principles.

The literature is full of speculations about various aspects of cochlear function and dysfunction. Unfortunately, we still do not have all the facts about many important issues. One of the most important examples of this is how the cochlea attains its sensitivity and frequency selectivity, which is very much a matter of opinion. A second important example is dynamic range (acoustic intensity) compression, due to the operation of cochlear outer hair cells (OHC).

However today our experimental knowledge is growing at an accelerating pace because of a much tighter focus on the issues. We now know that the answers to the questions of cochlear sensitivity, selectivity, and dynamic range, lie in the function of the outer hair cells. As a result, a great deal of attention is now being concentrated on outer hair cell biophysics.

This effort is paying off at the highest level. Three examples come to mind. *First* is multiband compression hearing aids. This type of signal processing, first proposed in 1938 by Steinberg and Gardner, has revolutionized the hearing aid industry in the last 10 years. With the introduction of compression signal processing, hearing aids work. This powerful circuit is not the only reason hearing aids of today are better. Better electronics and transducers have made impressive strides as well. In the last few years the digital barrier has finally been broken. One might call this the last frontier in hearing aid development.

A *second* example is the development of otoacoustic emissions (OAE) as a hearing diagnostic tool. Pioneered by David Kemp and Duck Kim, and then by many others, this tool allows for the cochlear evaluation of infants only a few days old. The identification of cochlear hearing loss at such an early stage is dramatically changing the lives of these children and their parents for the better. While it is tragic to be born deaf, it is much more tragic to not recognize the deafness until the child is 3 year old, when he or she fails to learn to talk. With proper and early intervention, these kids lead normal, productive lives.

A *third* example continues to evade us, namely how the auditory system, including the cochlea and the auditory cortex, processes human speech. If we can solve this grail-like problem, we will fundamentally change the way humans and computers interact, for the better. The ultimate hearing aid is the hearing aid with built in robust speech recognition. We have no idea when this will come to be, and it is undoubtedly many years off, but when it happens it will be a revolution that will not go unnoticed.

Chapter Outline: Several topics will be reviewed. First, the history of cochlear models, including extensions that have taken place in recent years. These models include both macromechanics and micromechanics of the tectorial membrane and hair cells. This leads to comparisons of the basilar membrane, hair cell, and neural frequency tuning. The role of nonlinear mechanics and dynamic range are covered to help the student understand the importance of modern wideband dynamic range compression hearing aids. Hearing loss, loudness recruitment, as well as other important topics of modern hearing health care, are briefly discussed.

This paper assumes a basic knowledge of cochlear anatomy. If the reader desires basic

knowledge about cochlear anatomy or function, many good text books exist that can fulfill that need better than this more advanced review paper [1, 2].

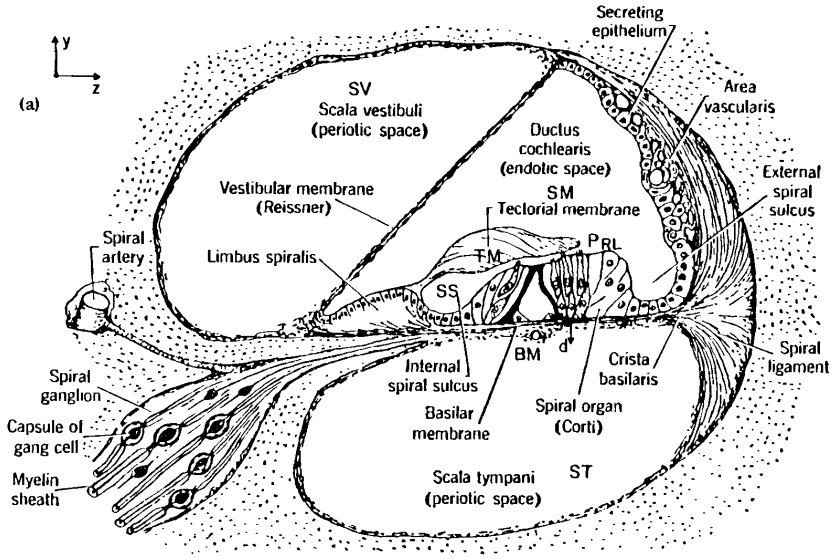

Figure 1: *Cross section through the cochlear duct showing all the major structures of the cochlea. The three chambers are filled with fluid. Reissner's membrane is an electrical barrier and is not believed to play a mechanical role.*

Function of the Inner Ear

The goal of cochlear modeling is to refine our understanding of how auditory signal are processed. Science is at its best as an interplay between experiment and theory. The two main roles of the cochlea are to separate the input acoustic signal into overlapping frequency bands, and to compress the large acoustic intensity range into the much smaller mechanical and electrical dynamic range of the inner hair cell. This is a basic problem of information processing by the ear. The eye plays a similar role as a peripheral organ. It breaks the light image into rod and cone sized pixels, as it compresses the dynamic range of the visual signal. Guided by the intensity JND, the corresponding visual dynamic range is about 9 to 10 orders of magnitude of intensity [3, 4], while the ear has about 11 to 12. Neurons are low bandwidth channels. The stimulus has a relatively high information rate. The eye and the ear must cope with this problem by reducing the stimulus to a large number of low bandwidth signals. It is then the job of the cortex to piece these pixel signals back together, to reconstruct the world as we see and hear it. This information coding starts in the organ of Corti, shown in Fig. 1. There are three major chambers, separated by Reissner's membrane and the basilar membrane (BM). However, mechanically speaking, there are two chambers, as Reissner's membrane is for electrical isolation of the Scala media (SM) [1, 2]. Figure 2 shows a blown up view of the organ of Corti where the inner hair cells (IHC) and outer hair cells (OHC) sit between the BM and the tectorial membrane (TM).

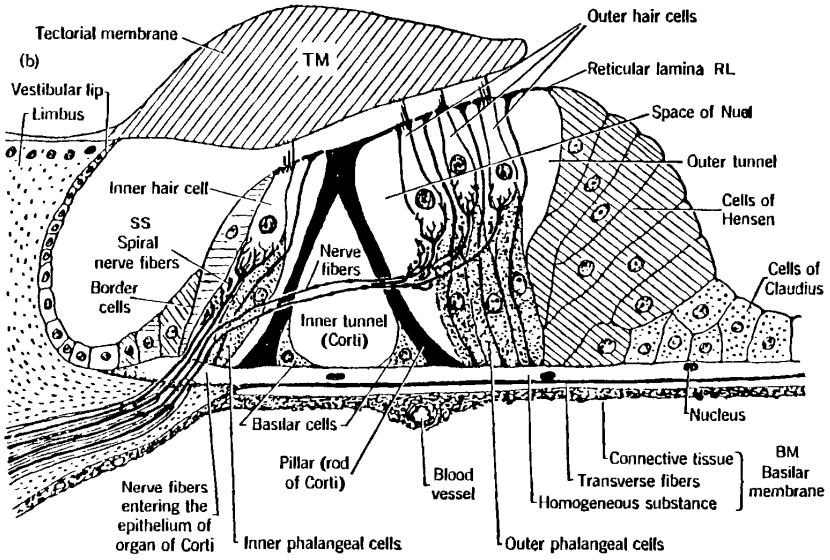

Figure 2: *This cross section of the Organ of Corti shows the inner and outer hair cells, pillar cells and other supporting structures, the basilar membrane (BM), and the tectorial membrane (TM).*

Inner Hair Cells. In very general terms, the role of the cochlea is to convert sound at the eardrum into neural pulse patterns along ≈30,000 neurons of the human auditory (VIIIth) nerve. After being filtered by the cochlea, a low level pure tone has a narrow spread of excitation which excites the cilia of about 40 contiguous inner hair cells. Cilia excitation is a narrow band signal with a center frequency that depends on the inner hair cell's location along the basilar membrane. Each hair cell is about 10 micrometers in diameter while the human basilar membrane is about 35 mm in length (35,000 microns). Thus the neurons of the auditory nerve encode the responses of about 3,500 inner hair cells which form a single row of cells along the length of the BM. Each inner hair cell voltage is a lowpass filtered representation of the detected inner hair cell cilia displacement [5]. Each hair cell is connected to many neurons. In the cat, for example,[1] approximately 15–20 neurons encode each of these narrow band inner hair cells with a neural timing code. It is widely believed that the neuron information channel between the hair cell and the *cochlear nucleus* is a combination of the mean firing rate and the relative timing between neural pulses (spikes). The mean firing rate is reflected in the loudness coding, while the relative timing carries more subtle cues, including for example pitch information and speech voicing distinctions.

Outer Hair Cells. As shown in Fig. 2 there are typically 3 (sometimes 4) outer hair cells (OHCs) for each inner hair cell (IHCs), leading to about 12,000 for the human cochlea. Outer hair cells are used for intensity dynamic range control. This is a form of nonlinear signal processing, not dissimilar to Dolby sound processing.[2] It is well known (as was first proposed by Lorente de No [7] and Steinberg and Gardner [8]) that noise damage of

[1] It is commonly accepted that all mammalian cochleae are similar in function. The frequency range of operation differs between species.

[2] I am told that this form of processing was inspired by cochlear function, and was in use long before it was patented by Dolby, in movie sound systems developed by Bell Labs in the 1930's and 1940's. Telephone speech

"nerve cells" (i.e., OHCs) leads to a reduction of dynamic range, a disorder clinically called *dynamic range recruitment*.

We may describe cochlear processing two ways. First in terms of the signal representation at various points in the system. Second, in terms of models. These models are our most succinct means of conveying the results of years of detailed and difficult experimental work on cochlear function. The body of experimental knowledge has been very efficiently represented (to the extent that it is understood) in the form of these mathematical models. When no model exists (e.g., because we do not understand the function), a more basic description via the experimental data is necessary. Several good books and review papers are available which make excellent supplemental reading [9, 1, 10, 11, 4, 12].

For pedagogical purposes the discussion is divided into five sections: Section 1 *Macromechanics* describes the fluid motions of the scalae and treats the basilar membrane as a dynamical system having mass, stiffness, and damping. Section 2 *Inadequacies of the* 1^d *model* describes the experimental data that characterizes the nonlinear cochlea. Section 3 *OHC Transduction*, describes the electromechanical action of the outer hair cell on the basilar membrane. Most important is the nonlinear feedback provided by the outer hair cell, leading to the dynamic range compression of the inner hair cell excitation. Section 4 *Micromechanics* describes the models of the motion of the Organ of Corti, the inner and outer hair cell cilia, the tectorial membrane, and the motion of the fluid in the space between the reticular lamina and the tectorial membrane. Much of this section has been adapted from an earlier article [13]. Finally in Sec. 5 we briefly summarize the entire paper.

A warning to the reader: Due to experimental uncertainty there is diverse opinion in the literature about certain critical issues. While there are many areas of agreement, this paper is directed on those more interesting controversial topics. For example, (a) it is very difficult to experimentally observe the motion of the basilar membrane in a fully functional cochlea; (b) questions regarding the relative motion of the tectorial membrane to other adjacent structures are largely a matter of conjecture. Some of these questions are best investigated theoretically. The experimental situation is improving as new techniques are being invented. As a result, a multitude of opinions exist as to the detailed function of the various structures.

On the other hand, firm and widely accepted *indirect* evidence exists on how these structures work. This indirect evidence takes on many forms, such as neuro- and psychophysical, morphological, electrochemical, mechanical, acoustical, and biophysical. All these diverse forms of "indirect" data may be related via models. Their value is not depreciated because of their indirect nature. In the end, all the verifiable data must, and will, coexist.

1 Macromechanics

Typically the cochlea is treated as an uncoiled long thin box, as shown in Fig. 3. This represents the starting point for the macromechanical models.

is similarly compressed [6].

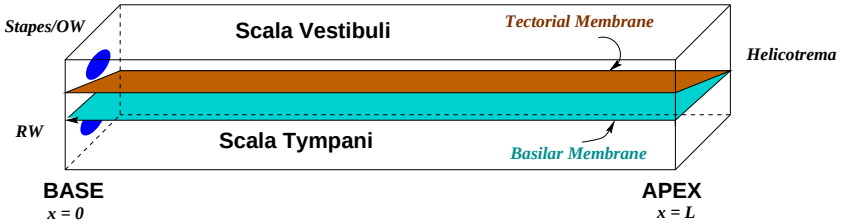

Figure 3: *Box model of the cochlea. The* Base *(x=0) is the high frequency end of the cochlea while the* Apex *($x = L$) carries the low frequencies.*

1.1 The early history of cochlear modeling.

I am told that Helmholtz's widely recognized model of the cochlea was first presented by him in Bonn in 1857 (subsequently published in a book on his public lectures in 1857 [14]), and again later in 1863 in chapter VI and in an appendix of *On the Sensations of Tone* [15]. Helmholtz likened the cochlea to a bank of highly tuned resonators, which are selective to different frequencies, much like a piano or a harp [14, page 22-58], with each string representing a different place on the basilar membrane. The model he proposed is not very satisfying however, since it left out many important features, the most important of which includes the cochlear fluid which couples the mechanical resonators together. But given the publication date, it is an impressive contribution by this early great master of physics and psychophysics.

The next major contribution, by Wegel and Lane (1924), stands in a class of its own even today, as a double barreled paper having both deep psychophysical and modeling insight.[3] The paper was the first to quantitatively describe the details of how a high level low frequency tone effects the audibility of a second low level higher frequency tone (i.e., the *upward spread of masking*). It was also the first publication to propose a "modern" model of the cochlea. If Wegel and Lane had been able to solve their model equations (of course they had no computer to do this), they would have predicted cochlear traveling waves. It was their mistake, in my opinion, to make this one paper. The modeling portion of their paper has been totally overshadowed by their experimental results.

I know of only two other early major works in cochlear modeling, one by Fletcher [17], and several by Ranke starting in 1931 (for a historical review see [18, 19]).

Contrary to some opinion [20], the significance of cochlear viscous fluid damping (a measure of the energy loss) was shown by Békésy to be very small [21, 22]. Fletcher's 1951 model [21] (Eq. 8) was the first to quantitatively consider fluid viscosity. In fact the inner ear is nearly a lossless system.[4] The significance of this is great. Imagine a nearly lossless bouncing ball. Such a ball would bounce wildly, similar to a "super ball." Low-loss structures, such as the cochlea, have unusual properties that appear to defy the laws of physics.

It was the experimental observations of G. von Békésy starting in 1928 on human cadaver cochleae which unveiled the physical nature of the basilar membrane traveling wave.

[3] Fletcher published much of the Wegel and Lane data one year earlier [16]. It is not clear to me why Wegel and Lane are always quoted for these results rather than Fletcher. In Fletcher's 1930 modeling paper, he mentioned that he was the subject in the Wegel and Lane study. It seems to me that Fletcher deserves some of the credit.

[4] Fletcher [21] page 639 clearly states this fact. This conclusion also follows from a calculation of the "viscous boundary layer thickness" relative to the scala dimensions [23]. At low frequencies, below a few hundred hertz, scalae damping is significant [21, 24, 25].

What von Békésy found (consistent with the 1924 Wegel and Lane model) was that the cochlea is analogous to a "dispersive" transmission line where the different frequency components which make up the input signal travel at different speeds along the basilar membrane, thereby isolating each frequency component at a different place along the basilar membrane. He properly named this dispersive wave a "traveling wave." He observed the traveling wave using stroboscopic light, in dead human cochleae, at sound levels well above the pain threshold, namely above 140 dB SPL.[5] These high sound pressure levels were required to obtain displacement levels that were observable under his microscope. von Békésy's pioneering experiments were considered so important that in 1961 he received the Nobel prize.

Over the intervening years these experiments have been greatly improved, but von Békésy's fundamental observation of the traveling wave still stand. His original experimental results, however, are *not* characteristic of the responses seen in more recent experiments, in many important ways. These differences are believed to be due to the fact that Békésy's cochleae were dead, and because of the high sound levels his experiments required.

Today we find that the traveling wave has a more sharply defined location on the basilar membrane for a pure tone input than observed by von Békésy. In fact, according to measurements made over the last 20 years, the response of the basilar membrane to a pure tone can change in amplitude by more than five orders of magnitude per millimeter of distance along the basilar membrane (i.e., 300 dB/oct is equivalent to 100 dB/mm in the cat cochlea).

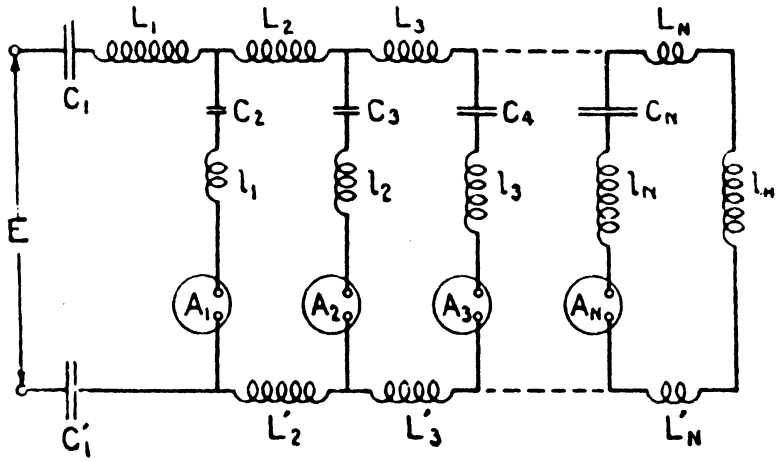

Figure 4: *Figure 7b from 1924 Wegel and Lane paper.*

To describe this response it is helpful to call upon the 1924 Wegel and Lane and the 1930 Fletcher model of macromechanics, *the transmission line model,* which was first quantitatively analyzed by J. J. Zwislocki (1948, 1950), Peterson and Bogart (1950), and Fletcher (1951). The transmission line model is also called the *one-dimensional* (1^d), or *long-wave* model.

[5] One dB corresponds to a 12% change.

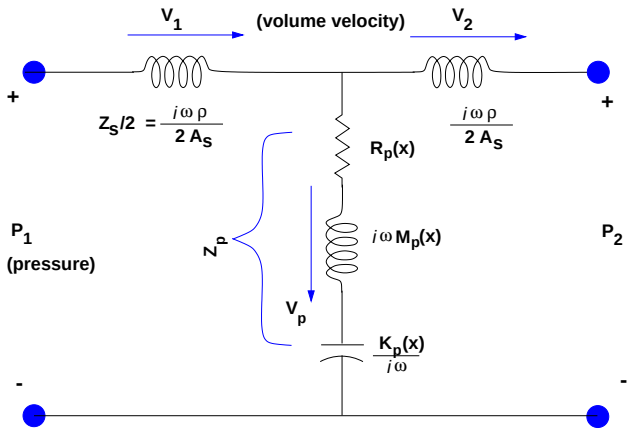

Figure 5: *A single section of the electrical network 1^d model described by Wegel and Lane. The model is built from a cascade of such section.*

1.2 The 1^d model of the cochlea

Zwislocki (1948) was first to quantitatively analyze Wegel and Lane's macromechanical cochlear model, explaining Békésy's traveling wave. Wegel and Lane's 1924 model is shown in Figs. 4 and 5. The stapes input pressure P_1 is at the left, with the input velocity V_1, as shown by the arrow, corresponding to the stapes velocity. This model represents the mass of the fluids of the cochlea as electrical inductors and the BM stiffness as a capacitor.Electrical circuit networks are useful when describing mechanical systems. This is possible because of an electrical to mechanical analog that relates the two systems of equations, and because the electrical circuit elements comprise a de facto standard for describing such equations. It is possible to write down the equations that describe the system from the circuit of Fig. 5, by those trained in the art. Engineers and scientists frequently find it easier to "read" and think in terms of these pictorial circuit diagrams, than to interpret the corresponding equations.

1.2.1 Impedance.

During the following discussion it is necessary to introduce the concept of a *1-port* (two-wire) impedance. Impedance is typically defined in the frequency domain in terms of pure tones $A\sin(2\pi ft + \phi)$, which is characterized by amplitude A, driving frequency f, and phase ϕ. *Ohm's Law* defines impedance as

$$\textit{Impedance} = \frac{\textit{effort}}{\textit{flow}}. \tag{1}$$

In an electrical system the impedance is the ratio of a voltage (effort) over a current (flow). In a mechanical system it is the force (effort) over the velocity (flow). I next give three important examples:

Example 1: The impedance of the tympanic membrane (TM, or eardrum) is defined in terms of a pure tone pressure in the ear canal divided by the resulting TM volume velocity (the velocity times the area of TM motion). The pressure (effort) and volume velocity (flow)

referred to here are conventionally described using complex numbers, to account for the phase relationship between the two.

Example 2: The impedance of a spring is given by

$$Z(f) = \frac{K}{2\pi i f}, \tag{2}$$

where K is the stiffness of the spring and f is the frequency. This element is represented as two straight lines (Fig. 5) close together, which looks like two physical plates. The important term

$$i = \sqrt{-1}, \tag{3}$$

in the denominator, indicates that the impedance of a spring has a phase of $-\pi/2$ (-90^o). This phase means that when the velocity is $\cos(2\pi f t)$, the force is $\sin(2\pi f t)$. The definition of Eq. 2 follows from *Hooke's Law* which says that the force F and displacement X of a spring are proportional, namely

$$F = KX. \tag{4}$$

Since the velocity $V = 2\pi i f X$, and the definition of the impedance is ratio of F/V, Eq. 2 follows.

Example 3: From *Newton's Law* $F = Ma$ where F is the force, M is the mass, and acceleration $a = 2\pi i f V$. The electrical element corresponding to a mass is an "inductor," indicated in Fig. 5 by a coil. Thus for a mass

$$Z(f) = 2\pi i f M. \tag{5}$$

From Eq.'s 2 and 5, the magnitude of the impedance of a spring decreases as $1/f$, while the impedance magnitude of a mass is proportional to f. The stiffness with its -90^o phase is called a *lagging* phase, while the mass with its +90^o phase is called a *leading* phase.

1.2.2 Thévenin equivalence

When dealing with impedance circuits there is a very important concept called the *Thévenin equivalent circuit*. In 1883 a French telegraph engineer Léon Thévenin showed[6] that any active 1-port circuit, of any complexity, is equivalent to a series combination of a *source voltage* V_s and a *source impedance* Z_s. These two elements are uniquely defined by performing two independent measurements. Any two independent measurements would do, but for the purpose of definition, two special measurements are best. The first defines V_s, which is called the *open circuit* voltage. This is the voltage measured with *no load* on the system. The second measurement is the *short circuit* (*unloaded*) current I_s, defined as the current when the two terminals are connected together. By taking the ratio of the open circuit voltage and the short circuit current, the Thévenin impedance is obtained $Z_s = V_s/I_s$.

The classical example is a battery. The open circuit voltage defines the Thévenin voltage V_s, which is the voltage measured with no load. The short circuit current I_s is the current measured with a wire across the terminals (don't try this!). The Thévenin impedance $Z_s \equiv V_s/I_s$ is the unloaded voltage divided by the short circuit current.

As a second example consider an earphone. When unloaded, by placing the earphone in a very small cavity so that it has very little air to move, it can produce an "open circuit" pressure. However, when loaded by placing it in the ear canal, the earphone pressure is

[6] Apparently Helmholtz worked this result out even earlier.

reduced, due to the load of the ear canal. If it were placed in water, the load would be very large, and the corresponding pressure would be small. In this case the "short circuit current" corresponds to volume velocity of water that the diaphragm of the earphone can move. The Thévenin parameters are the pressure measured in the small cavity, and the impedance defined by the Thévenin pressure divided by the volume velocity measured when place in in the water load.

The Thévenin parameters are needed to characterize a hair cell's properties.

1.3 2-port analysis

The concept of a 1-port impedance and of a Thévenin equivalence circuit has been generalized by defining a *2-port* (4-wire connection) [30]. This is a very important modeling tool that is used every time we must deal with both an input and an output signal. This methodology is called *2-port* analysis by engineers [31, 30, 32], referring to the fact that a transducer has an input and output. A related literature is called *Bond Graph* analysis [33]. A pair of "impedance" (conjugate) variables *effort* and *flow* (see section Sec. 1.2.1 and [31]), are used in each of two domains, the input and the output, to characterize the transducer.

The 2-port relation properly characterizes the relations between an input effort and flow, which we denote as lower case variables e, f, and an output effort and flow, characterized by upper case variables E, F. This characterization is in the frequency domain, and it requires four functions of complex frequency $s \equiv i2\pi$frequency, which are traditionally called $A(s), B(s), C(s), D(s)$ [30]. These four functions completely characterize the linear 2-port. Complex frequency s is the necessary frequency variable for functions that are *causal* (one sided in time), as in the case of impedances.

$$\begin{bmatrix} E \\ F \end{bmatrix} = \begin{pmatrix} A(s) & B(s) \\ C(s) & D(s) \end{pmatrix} \begin{bmatrix} e \\ f \end{bmatrix}, \tag{6}$$

In later sections we shall see that all of the impedance and Thévenin properties are captured in this one *matrix* equation. A 2-port is called *reciprocal* if it is reversible. For reciprocal systems,

$$AD - BC = 1. \tag{7}$$

If a system is reciprocal then it is *bidirectional* because when the determinant of the $ABCD$ matrix is 1 (Eq. 7), the inverse system must exist.

Each section of the the Wegel and Lane model Fig. 5. has a series impedance Z_s and a shunt impedance Z_p. Thus it is a cascade of three $ABCD$ matrices, which may be written as

$$\begin{bmatrix} P_1 \\ V_1 \end{bmatrix} = \begin{bmatrix} 1 & Z_s/2 \\ 0 & 1 \end{bmatrix} \begin{bmatrix} 1 & 0 \\ 1/Z_p & 1 \end{bmatrix} \begin{bmatrix} 1 & Z_p/2 \\ 0 & 1 \end{bmatrix} \begin{bmatrix} P_2 \\ V_2 \end{bmatrix}, \tag{8}$$

This provides a mathematical formulation of a section of the Wegel and Lane model. The details for doing this are derived in Pipes [30].

If the system is reversed and its topology is identical then, $B = C$. This is called a *symmetric* network, which is a common special case of a reciprocal 2-port. For example, Figure 5 is symmetric when the scala area is constant.

Reciprocal systems. The classic example of a reciprocal network is a piezoelectric crystal, while the classic example of a non reciprocal network is a transistor. More to the point, outer hair cell *forward transduction*, which characterizes the relation between the cell's cilia displacement (the input) and the cell's membrane voltage (the output), is typically characterized as non-reciprocal. *Reverse transduction*, which characterizes the membrane voltage (the input) and the output motility (the output) is believed (but not yet proven) to be reciprocal.

1.3.1 Anatomy of the model.

Different points along the basilar membrane are represented by the cascaded sections of the transmission line model of Fig. 5. The position along the model corresponds to the longitudinal position along the cochlea. The series (horizontal) inductors (coils) represent the fluid mass (inertia) along the length of the cochlea, while the elements connected to ground (the common point along the bottom of the figure) represent the mechanical (acoustical) impedance of an element of the corresponding section of the basilar membrane. In the Wegel and Lane model the partition impedance, defined as the pressure drop across the basilar membrane divided by its volume velocity per unit length, has the form

$$Z_p(f,x) = K_p(x)/s + R_p(x) + sM_p(x), \tag{9}$$

where R_p is the resistance. Each inductor going to ground represents the partition and fluid mass per unit length $M_p(x)$ of the section, while the capacitor represents the compliance [the reciprocal of the stiffness $K_p(x)$] of the section of basilar membrane. Note that sM and K/s are impedances, but M is simply a mass, and K a stiffness, but not an impedance. The stiffness decreases exponentially along the length of the cochlea, while the mass is frequently approximated as being independent of position. The position variable x is frequently called the *place* variable.

Driving the model To understand the inner workings of Wegel and Lane's circuit Fig. 5, assume that we excite the line at the stapes with a sinusoidal velocity of frequency f. Due to conservation of fluid mass within the cochlea (fluid mass cannot be created or destroyed in this circuit), at every instant of time the total volume through the basilar membrane must equal the volume displaced by the stapes. Simultaneously, the round window membrane, connected to the scala tympani, must bulge out by an equal amount [34]. In practice the motion of the basilar membrane is complicated. However the total volume displacement of the basilar membrane, at any instant of time, must be equal to the volume displacement of the stapes, and of the round window membrane.

Flow in the model. Consider next where the fluid current V_1 will flow, or where it can flow. As shown in Fig. 6, for a given input frequency the basilar membrane impedance magnitude has a minimum at one point along the length of the cochlea. The physical meaning of this is that there is one point along the membrane that can move in a relatively unrestricted manner. The location of this point critically depends on frequency. The impedance being described is the impedance of each group of three elements in series in Fig. 5, namely the inductor-capacitor-resistor combination going to ground at each point along the length of the cochlea. These three elements in this configuration have special significance because at one frequency the impedance of the inductor and the capacitor cancel each other, and

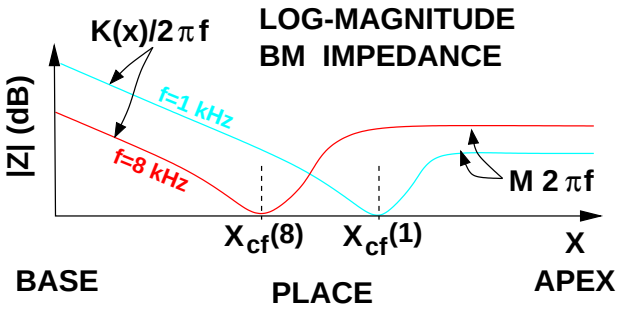

Figure 6: *Plot of the log-magnitude of the impedance as a function of place for two different frequencies of 1 and 8 kHz. The region labeled $K(x)$ is the region dominated by the stiffness and has impedance $K(x)/s$. The region labeled M is dominated by the mass and has impedance sM. The characteristic places for 1 and 8 kHz are shown as X_{cf}.*

the only impedance element that contributes to the impedance is the resistance. This point is called the *resonant point*, which is defined as that frequency F_{cf} where the mass and stiffness impedance are equal

$$\frac{K(x)}{2\pi i F_{cf}} = 2\pi i F_{cf} M. \tag{10}$$

Solving for $F_{cf}(x)$ defines the *cochlear map function*, which is one of the most important concepts of cochlear modeling

$$F_{cf}(x) \equiv \frac{1}{2\pi}\sqrt{K_p(x)/M_p}. \tag{11}$$

The inverse of this function $X_{cf}(f)$ specifies the location of the "hole" shown in Fig. 6 as a function of frequency.

Basal to the resonant point $X_{cf}(f)$ of Fig. 6, the basilar membrane is increasingly stiff (has a large capacitive impedance), and apically (to the right of the resonant point), the impedance is a large mass reactance (inductive impedance). In this apical region the impedance is largely irrelevant since little fluid will flow past the mechanical hole labeled X_{cf} at the minimum. The above description is dependent on the input frequency f since the location of the hole (the impedance minimum) is frequency-dependent.

This description is helpful in our understanding in why the various frequency components of a signal are splayed out along the basilar membrane. If we were to put a pulse of current in at the stapes, the highest frequencies that make up the pulse would be shunted close to the stapes, while the lower frequencies would continue down the line. As the pulse travels down the basilar membrane, the higher frequencies are progressively removed, until almost nothing is left when the pulse reaches the right end of the model (the helicotrema end, the apex of the cochlea).

Let's next try a different mental experiment with this model. Suppose that the input at the stapes were a slowly swept tone or chirp. What would the response at a fixed point on the basilar membrane look like at one point along the basilar membrane? The ratio of the displacement BM to stapes displacement, as a function of frequency f, has a shallow low frequency slope and a very sharp high frequency slope. This response describes a lowpass filter.

Derivation of the cochlear map function. The cochlear map function $F_{cf}(x)$ plays a very important role in cochlear mechanics, has a long history, and is known by many names [17, 35, 36, 37, 38, 39]. The following derivation for the form of the cochlear map, based on "counting" critical bands, is from Fletcher [40] and Greenwood [39]. The *number of critical bands* $N_{cb}(x)$ may be found by integrating the density of critical bandwidth over frequency in *Hz* $\Delta_f(f)$ and over place $\Delta_x(x)$ in *mm*. The cochlear map function $F_{cf}(x)$ is then found by equating these two integrals.

The *critical bandwidth* $\Delta_f(f)$ is the effective width in frequency of the spread of energy on the basilar membrane. It has been estimated by many methods. The historical methods used by Fletcher were based on the critical ratio $\kappa(f)$ and the pure tone *just noticeable difference* in frequency (JND$_f$). These two psychoacoustic measures have a constant ratio of 20 between them [36] and page 171 of [41], namely the critical bandwidth in Hz equals 20 JND$_f(f)$ in Hz. From [17] (Eq. 6)

$$\log_{10}[\text{JND}_f(x)] = \frac{16 - x}{16.6} + 3, \tag{12}$$

with x in mm. Thus the *critical ratio* (in dB) $\kappa_{dB}(x)$ is of the form $ax + b$ where a and b are constants. The critical bandwidth, converted back to Hz, is

$$\Delta_f(x) = 10^{\kappa_{dB}(x)/10}. \tag{13}$$

This was verified by Greenwood [39], page 1350, Eq. 1.

The critical spread $\Delta_x(x)$ is the effective width of the spread of energy on the basilar membrane due to a pure tone. Based on an argument of Fletcher's, Allen found that in the cat $\Delta_x(x)$ corresponds to about 2.75 times the width of the basilar membrane $W_{bm}(x)$ [40], namely

$$\Delta_x(x) = 2.75 W_{bm}(x). \tag{14}$$

The two ratio measures $df/\Delta_f(f)$ and $dx/\Delta_x(x)$ define the density of critical bands in frequency and place, and each may be integrated to find the number of critical bands $N_{cb}(x)$. Equating these two functions results in the cochlear map function $F_{cf}(x)$

$$N_{cb}(x) \equiv \int_0^x \frac{dx}{\Delta_x(x)} = \int_0^{F_{cf}} \frac{df}{\Delta_f(f)}. \tag{15}$$

For a discussion of work after 1960 on the critical band see [40, 12].

Cochlear map in the Cat In 1982 Liberman [42] and in 1984 Liberman and Dodds [43] directly measured $F_{cf}(x)$ in the cat and found the following empirical formula

$$F_{cf}(x) = 456\left(10^{2.1x} - 0.8\right), \tag{16}$$

where the "place" variable x is normalized by the length of the basilar membrane, and is measured from the stapes [42]. As defined in Fig. 7, the "slope" of the cochlear map, which for the cat is 3 mm/oct and for the human is 5 mm/oct, is determined by the parameter 2.1 in the exponent of Eq. 16.

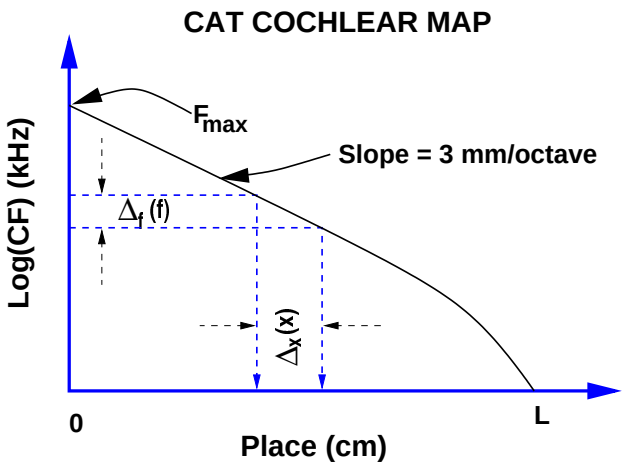

Figure 7: *Cochlear map of the cat following Liberman and Dodds, Eq. 16. This figure also shows how a critical band $\Delta_f(f)$ and a critical spread $\Delta_x(x)$ area related through the cochlear map function.*

2 Inadequacies of the 1^d model (Summary of experimental data)

Wegel and Lane's transmission line model was a most important development, since it was a qualitative predictor (by 26 years) of the experimental results of von Békésy, and it was based on a simple set of physical principles (conservation of fluid mass, and spatially variable basilar membrane stiffness). The Wegel and Lane 1^d model was the theory of choice until the 1970's when:

- numerical model results became available, which showed that 2^d and 3^d models were more frequency selective than the 1^d model,
- experimental basilar membrane observations showed that the basilar membrane motion had a nonlinear compressive response growth, and
- improved experimental basilar membrane observations became available which showed increased nonlinear cochlear frequency selectivity.

In the next section we review these developments.

2.1 Contemporary history of cochlear modeling

In 1976 George Zweig and colleagues pointed out that an approximate but accurate solution for the 1^d model could be obtained using a well known method in physics called the "WKB" approximation [44]. The method was subsequently widely adopted [45]. The results of Zweig *et al.* were similar to Rhode's contemporary basilar membrane data [46], but very different than contemporary neural tuning curve responses [47].[7]

[7] Of course Zweig's model was linear, and both Rhode's and Kiang and Moxon's data exposed significant nonlinear behavior.

The discrepancy in frequency selectivity between basilar membrane and neural responses has always been, and still is, the most serious problem for the cochlear modeling community. *In my view, this discrepancy is one of the most basic unsolved problems of cochlear modeling.* Progress on this front has been seriously confounded by the uncertainty in, and the interpretation of, the experimental data. We shall soon return to this same point.

2^d models: The need for a two-dimensional (2^d) theory was first explicitly presented by Ranke [18]. In the 70's several 2^d model solutions[8] became available [48, 49, 50, 51, 52]. These results made it clear that the 1^d theory, while a useful approximation, must be used only with cautioned thoughtful care.

Soon it was possible to compute the response of a 2^d, and even the response of a 3^d geometry [53, 45, 54]. As the complexity of the geometry of the models approached the physical geometry, the solutions tended to display steeper high frequency slopes, and therefore increased frequency selectivity. However, they did not converge to the neural responses.

A paradigm shift. Over a 15 year period starting in 1971, there was a paradigm shift. Three discoveries rocked the field:

a) nonlinear compressive basilar membrane and inner hair cell responses [46, 55],

b) otoacoustic emissions [56], and

c) motile outer hair cells [57].

Of course today we know that these observations are related, and all involve outer hair cells. A theory (a computational model) was desperately needed to tie all these results together (as it is today).

As the basilar membrane experimental measurements were refined, the experimental results exhibited increased cochlear frequency selectivity [58]. Inner hair cell recordings showed that these cells were tuned like neurons [55, 59]. The similarity of the inner hair cell recordings to neural responses is striking. Besides the increased tuning, Rhode's 1978 observations strongly supported much earlier indirect observations which suggested that nonlinearity played a fundamental role in cochlear mechanics [60, 61, 62, 63, 64].

Initially Rhode's discovery of basilar membrane nonlinearity was not widely accepted, and the frequency selectivity question was the more important issue. Contemporary experiments were geared at establishing the transformation between basilar membrane and neural tuning [65]. This was the era of the "second filter." There were some important theoretical second filter results [64, 66, 67, 68] addressing the gap between the BM and neural frequency response.

By 1982 strong controversial claims were being made that the basilar membrane frequency response (the selectivity) was similar to neural and inner hair cell data [69, 70]. Both authors soon modified their claims. Khanna reported the very strange result that the best frequency of tuning was correlated to the distance between the microphone and the ear drum [71]. The obvious, and now accepted explanation for this correlation, is that

[8] The 2^d theories are more rigorous than the 1^d theory, and therefore are a check on the simpler models. Any discrepancy must be attributed to the simpler 1^d theory.

standing wave reflections from the middle ear created a deep null in the ear canal pressure. This pressure was then used as a normalization of the basilar membrane displacement response. Thus the pressure null produced a large peak in the resulting incus displacement to ear canal pressure transfer function.

Sellick *et al.* (1983) reviewed their 1982 data and cryptically concluded

> "In conclusion, a demonstration of inner hair cell tuning at the level of the basilar membrane continues to elude us."

They went much further by showing how the size and placement of the Mössbauer source significantly influenced basilar membrane tuning [73].

On the theoretical side it was becoming clear that even a 3^d model, no matter how much more frequency selective it was compared to the 1^d model, would not be adequate to describe either the newly measured selectivity, or the neural tuning. The main difference was the tuning slope S_2 just below F_{cf}, which will next be described when we discuss Fig. 9.

Summary: An important consequence of Sellick's 1983 and Khanna's 1986 papers was that all the basilar membrane tuning results prior to 1986, with the possible exception of Rhode's, were in serious doubt. Equally important, it was a major problem that there was no accepted available theory that could predict the observations of either the basilar membrane nonlinearity, frequency selectivity, or the hair cell and neural tuning.

It was during this uncertain period that David Kemp observed the first otoacoustic emissions (tonal sound emanating from the cochlea and nonlinear "echos" to clicks and tone bursts) [56, 74, 75, 76, 77]. Kemp's findings were like an electric jolt to the field.

It was an exciting time, but the field was becoming chaotic due to the infusion of new results. It would take 20 or more years to clarify the situation, and require at least one more major discovery. In 1985 Brownell and colleagues discovered that the outer hair cell is motile [57].

Brownell's finding fundamentally changed the experimental landscape as researchers focused on outer hair cell experiments rather than on the basilar membrane itself. These results would pave the way toward explaining both the purpose and nonlinear operation of the mysterious outer hair cell.

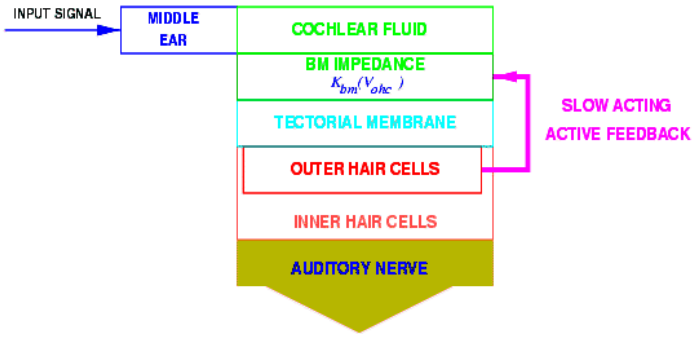

Figure 8: *Block flow diagram of the inner ear [78].*

The OHCs are the one common element that link all the nonlinear data previously observed, and a missing piece of the puzzle that needs to be understood, before any model

can hope to succeed in predicting basilar membrane, hair cell, and neural tuning, and nonlinear compression. Understanding the outer hair cell's two-way mechanical transduction is viewed as the key to solving the problem of cochlear dynamic range.

In the last year a fourth important discovery has been made. It has been shown that the outer hair cell mechanical stiffness depends on the voltage across its membrane [79, 80]. This change in stiffness, coupled with the naturally occurring "internal" turgor pressure, may well account for the voltage dependent accompanying length changes (the cell's voltage dependent motility). This leads to a block diagram feedback model of the organ of Corti shown in Fig. 8 where the excitation to the OHC changes the cell voltage V_{ohc}, which in turn changes the basilar stiffness [78].

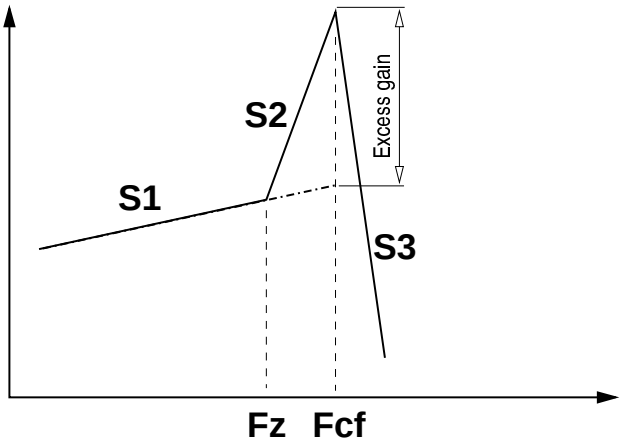

Figure 9: *Their are 6 numbers that characterize every curve, three slopes (S_1, S_2, S_3), in dB/oct, and two frequencies (F_z, F_{cf}). Finally the* excess gain *characterizes the amount of gain at F_{cf} relative to the gain defined by S_1. The Excess gain frequently depends on the input level for the case of a nonlinear response like the cochlea.*

2.1.1 Measures of cochlear response

There are two basic intertwined problems, *cochlear frequency selectivity* and *cochlear nonlinearity*. Whenever scientists are confronted with tangling (statistically correlated and complex) phenomenon, good statistical measures are crucial. A measure called Q_{10} has been popular, defined as the center frequency F_{cf} divided by the bandwidth measured 10 dB down from the peak. This measure is exquisitely insensitive to many important details and is difficult to accurately measure. Computing the bandwidth 10 dB down is subject to the error in estimating both the peak magnitude and the bandwidth. To compute Q_{10}, one must subtract these two estimates, and then divide by this small quantity. Such manipulations are prone to large errors.

An alternative measure due to Rhode [58, Fig. 8], and defined here in Fig. 9, is used in this review. Tuning curves are fitted by straight lines on log-log coordinates. Such straight line fits are called *Bode plots* in the engineering literature. The *slopes* and *break points*, defined as the locations where the straight lines cross, characterize the response. This measure is robust because it is a global measure of the response rather than a local measure (like Q_{10}). We shall provide these numbers when making comparisons of data from

the literature.

Such *Bode plots* are useful for characterizing both cochlear selectivity and nonlinearity. By looking at the slope difference $S_2 - S_1$ (see Fig. 9 for the definitions of the slopes), we have a statistic that is insensitive to the middle ear response. The slopes can be converted into the place domain by use of the cochlear map function. For example, in the cat where the conversion factor is 3 mm/oct, a slope of 6 dB/oct in the frequency domain is equivalent to 2 dB/mm. (The corresponding conversion factor for the human cochlea is 5 mm/oct.)

2.2 The nonlinear cochlea

Wegel and Lane's transmission line theory is linear. Researchers began studying ways of making the cochlear models nonlinear in order to better understand these numerous nonlinear effects. Because these models are still under development (since the problem has not yet been solved), it is necessary to describe the data rather than the models.

Some of these important nonlinear cochlear measures include:

- Distortion components generated by the cochlea, described by Wegel and Lane [81], Goldstein and Kiang [61], Smoorenburg [62], Kemp [75], Kim et al. [82], Fahey and Allen [83] (and many others),
- The upward spread of masking (USM), first described quantitatively by Wegel and Lane in 1924,
- Loudness growth and recruitment in the impaired ear [8],
- The frequency dependent neural two–tone suppression observed by Sachs and Kiang [84], Arthur *et al.* [85], Kiang and Moxon [47], Abbas and Sachs [86], Fahey and Allen [83], [87] and others,
- The frequency dependent basilar membrane response level compression first described by Rhode [46, 58], and,
- the frequency dependent inner hair cell receptor potential level compression, first described by Russell and Sellick [55, 59].

The following sections review these data.

2.2.1 The basilar membrane nonlinearity

The most basic of these nonlinear effects was first observed by Rhode [46, 58] when he measured the response of the basilar membrane, as shown in Fig. 10. He found the basilar membrane displacement to be a highly nonlinear function of level. For every four dB of pressure level increase on the input, the output displacement (or velocity) only changed one dB. This compressive nonlinearity depends on frequency, and only occurs near the most sensitive region (e.g., the tip of the tuning curve). For other frequencies the system was linear, namely, one dB of input change gave one dB of output change for frequencies away from the best frequency. This nonlinear effect was highly dependent on the health of the animal, and would decrease, or would not be present at all, if the animal was not in its physiologically pristine state. From Fig. 10 Rhode found up to $\approx$35 dB of excess gain at 7.4 kHz and 55 dB SPL, relative to the gain at 105 dB SPL. From of the 50 dB SPL curve of

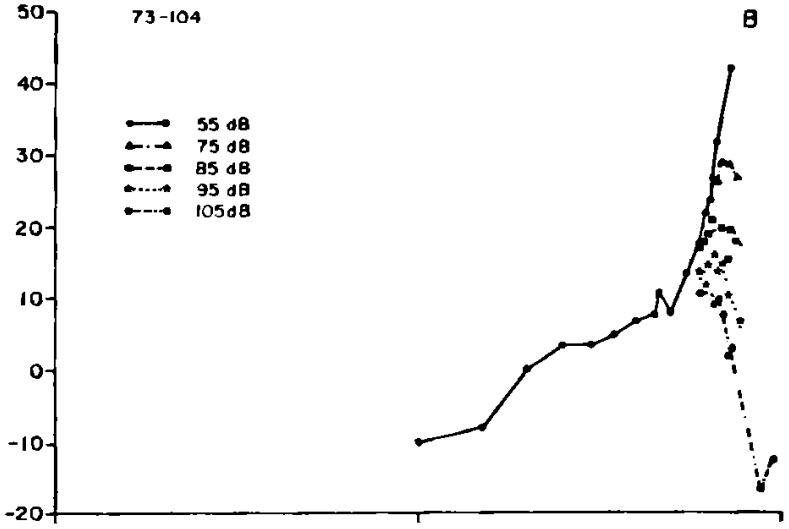

Figure 10: *Figure 9a, panel B from Rhode (1978) showing the response of the basilar membrane for his most sensitive animal. The graduals along the abscissa are at 0.1, 1.0 and 10.0 kHz.*

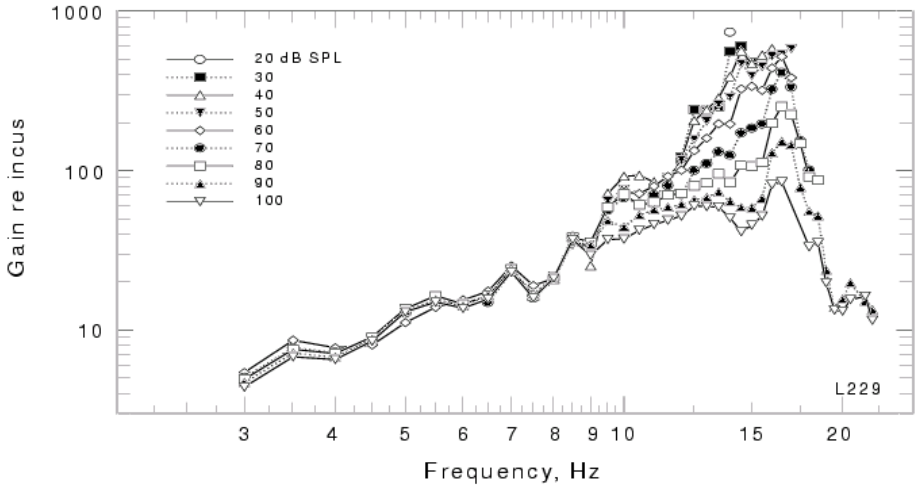

Figure 11: *Response of the basilar membrane in the* hook *region, 1.5 mm from the end as reported by Narayan and Ruggero [88]. These data are reported to be slightly less sensitive than data taken 3 mm from the end of the basilar membrane by the same laboratory.*

DATA TYPE	Reference	$\log_2(F_{cf}/F_z)$ octave	S1 dB/oct	S2 dB/oct	S3 dB/oct	Ex. Gain dB
BM	[58]	0.57	9	92	107	27
BM	[88]	0.88	10	30	101	17.4
Neural $F_{cf} > 3$ (kHz)	[90]	0.5–0.8	0–10	50–170	> 300	50–80

Table 1: *Summary of the parametric representation of basilar membrane (BM) and neural tuning from various sources. The parameters are defined in Fig. 9.*

Fig. 10 (the most sensitive case), and his Table I, $S_1 = 9$, $S_2 = 86$, and $S_3 = -288$ (dB/oct) (see Fig. 9 for the definitions), F_z = 5 kHz, F_{cf} = 7.4 kHz, and an *excess gain* of 27 dB. (Rhode reported S_1 = 6 dB/oct, but 9 seems to be a better fit to the data, so 9 dB/oct is the value we have used for our comparisons in Tab. 1.)

Very recent basilar membrane data from Narayan and Ruggero are shown in Fig. 11. In this figure we clearly see the nature of the nonlinear response growth and the change in frequency selectivity with input level.[9] For this figure $S_1 = 10$ dB/oct between 0.3 and 9.0 kHz, while S_2 for the 20 dB SPL curve between 9.0 and 15.0 kHz is slightly less than 30 dB/oct, S_3 = -101 dB/oct, F_z = 9 kHz, F_{cf} = 16.6 kHz, and the excess gain is 20 $\log$(600/80) = 17.4 dB.

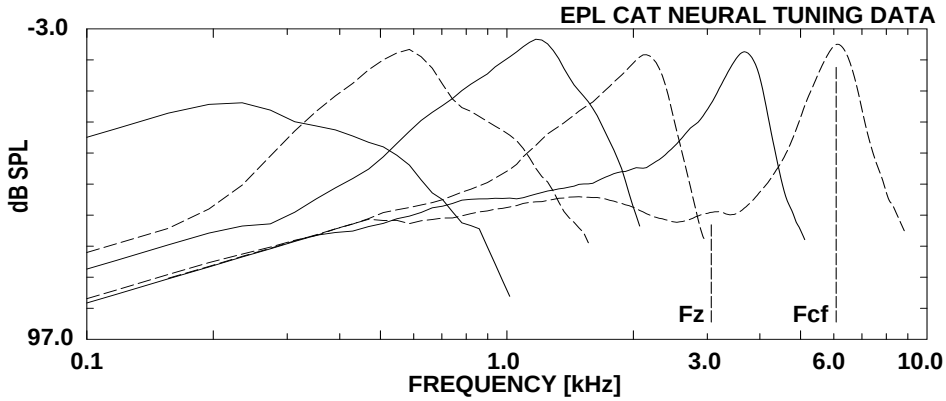

Figure 12: *Cat neural tuning curves from Eaton Peabody Lab provided by C. Liberman and B. Delgutte. The pressure scale, in dB, has been reversed to make the curves look like filter transfer functions. The response "tail" for the 6 kHz neuron is the "flat" region between 0.1 kHz and frequency F_z. In the tail the sound must be above 65 dB SPL (which on this scale is down) before the neuron will respond.*

2.2.2 Neural Tuning Data.

We ultimately seek a model which accurately predicts human inner hair cell and neural tuning curves. A great deal of cat VIIIth neural tuning curve data are available which defines fairly precisely the input-output properties of the cochlea at threshold intensities.

[9] Basilar membrane experiments are notoriously difficult. The variability across (and even within) laboratories is typically quite large [89].

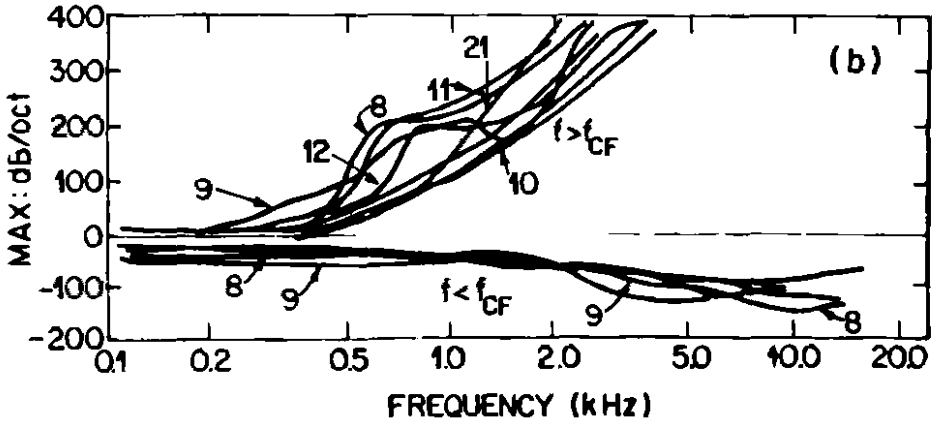

Figure 13: *Slopes of neural tuning curves for 8 different cats. The upper positive slopes, labeled $f > F_{cf}$ give S_3, the steep high frequency side of the tuning curve, while the negative slopes labeled $f < F_{cf}$ correspond to S_2, the slope in the range of frequencies $F_z < f < F_{cf}$. Above 2 kHz S_2 varies from 50 to more than 100 dB/oct, while S_3 varies from about 50 dB/oct at 0.5 kHz to more than 400 dB/oct above 2-3 kHz. The numbers on each curve code different animals. This figure is Fig. 3 of reference [90].*

Neural tuning is measured by measuring the spiking activity in an auditory nerve fiber as a function of the frequency and intensity of a probe search tone. The locus of threshold intensities $I_p^*(f_p)$ that cause the neuron to fire slightly above its spontaneous rate is called the *neural tuning curve*. The $*$ superscript indicates that the probe intensity is at threshold. Each neuron has such a tuning curve, which is tuned to its "best" characteristic frequency, labeled in Fig. 12 as F_{cf} and given by F_{cf} in Eq. 11. The tuning curves of Fig. 12 have been vertically reversed to make them look more like the *filter transfer functions* used in basilar membrane response plots.

Tuning curve slopes. Those tuning curves having best frequencies F_{cf} above a few kHz typically have "flat tails," meaning the broad flat region labeled as S_1 in Fig. 9 is less than 10 dB/oct. As an example look to the left of the frequency labeled Fz for the 7 kHz neuron of Fig. 12. For high frequency neurons ($F_{cf} > 2$ kHz), the slope in the tail $S_1 \approx 0$. It is shown in Fig. 13, S_2 is between 50-150 dB/oct, $|S_3| > 300$ dB/oct [90]. The excess gain is between 50-80 dB, and $F_{cf}/F_z \approx 0.5$ oct [91].

Tuning curve tips. Around the sensitive tips of tuning curves we expect the response to be similar to basilar membrane tuning, and there is significant evidence that this is the case [92, 88].

2.2.3 The receptor potential nonlinearity

In 1978 Russell and Sellick [55, 59] found a frequency dependent compressive nonlinear effect in the receptor potential of the inner hair cell of their guinea pig preparation. These independent measures of compressive nonlinearity, at a different point in the system, increased the credence of the hypothesis that the basilar membrane response is inherently

nonlinear, especially at low sound pressure levels. They also greatly strengthened and clarified the case for the two–tone suppression nonlinearity observed in neural responses [84, 47, 86] which, due to neural saturation effects, was more difficult to quantify.

2.2.4 Motile OHCs

The implication that hair cells might play an important role in cochlear mechanics go back at least two 1936 when loudness recruitment was first reported by Fowler [93] in a comment by R. Lorente de No. [7], stating that cochlear hair cells are likely to be involved in loudness recruitment.

The same year Steinberg and Gardner (1937) were explicit about the action of recruitment when they concluded

> When someone shouts, such a deafened person suffers practically as much discomfort as a normal hearing person would under the same circumstances. Furthermore for such a case, the effective gain in loudness afforded by amplification depends on the amount of variable type loss present. Owing to the expanding action of this type of loss it would be necessary to introduce a corresponding compression in the amplifier in order to produce the same amplification at all levels.

Therefore as early as 1937 there was a sense that cochlear haircells were related to dynamic range compression.

In more recent years, theoretical attempts to explain the difference in tuning between normal and damaged cochleae led to the suggestion that OHCs could influence BM mechanics. In 1983 Neely and Kim conclude

> We suggest that the negative damping components in the model may represent the physical action of outer hair cells, functioning in the electrochemical environment of the normal cochlea and serving to boost the sensitivity of the cochlea at low levels of excitation.

Subsequently, Brownell *et al.* (1985) discovered that isolated OHCs change their length when placed in an electric field [57]. This then lead to the intuitive and widespread proposal that outer hair cells act as linear motors that directly drive the basilar membrane on a cycle by cycle basis. As summarized in Fig. 8, the length change was shown to be controlled by the outer hair cell receptor potential, which in turn is modulated by both the position of the basilar membrane (forming a fast feedback loop), and alternatively by the efferent neurons that are connected to the outer hair cells (forming a slow feedback loop). The details of this possibility are the topic of present research.

2.2.5 Low frequency suppressor effects

The psychophysically measured *upward spread of masking* (USM) and the neurally measured *two-tone suppression* (2TS) are closely related phenomena. Unfortunately these two measures have been treated independently in the literature. Today we know that they are alternative objective measures of the same OHC compressive nonlinearity. The USM is measured psychophysically while 2TS is a neural measure. Both involve the suppression of a basal (high frequency) probe due to the simultaneous presentation of an apical (low

frequency) suppressor. These two views (USM versus 2TS) nicely complement each other, providing a symbiotic view of cochlear nonlinearity.

Upward Spread of Masking (USM). In a classic 1876 paper [95, 96], A.M. Mayer, was the first to describe the asymmetric nature of masking. Mayer made his qualitative observations with the use of organ pipes and tuning forks, and found that that the spread of masking is a strong function of the probe-to-masker frequency ratio (f_p/f_m).

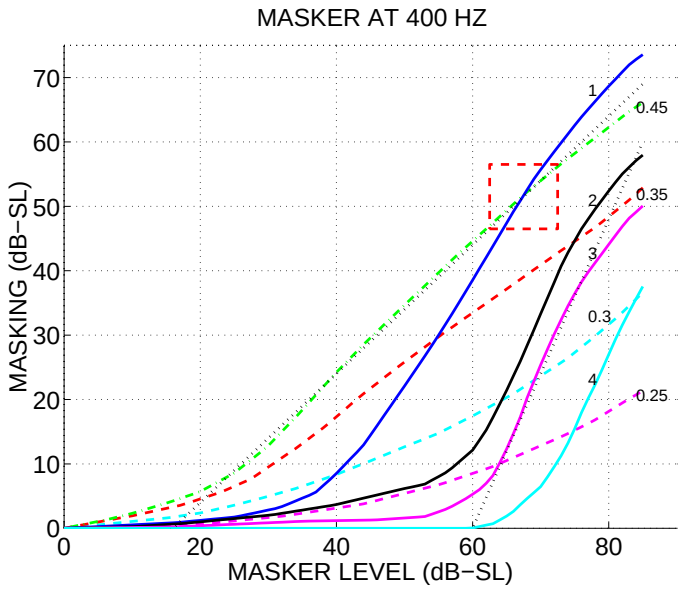

Figure 14: *Masking from Wegel and Lane using a 400 Hz masker. The abscissa is the masker intensity I_m in dB-SL. The ordinate is the threshold probe intensity $I_p^*(I_m)$ in dB-SL. The frequency of the probe f_p, expressed in kHz, is the parameter indicated on each curve.*

In 1923, Fletcher published the first quantitative results of tonal masking.[10] In 1924, Wegel and Lane extended Fletcher's experiments (Fletcher was the subject [17, Page 325]), using a wider range of tones. Wegel and Lane then discuss the results in terms of their 1^d model described above. As shown in Fig. 14, Wegel and Lane's experiments involved presenting listeners with a masker tone at frequency f_m and intensity I_m, along with a probe tone at frequency f_p. As a function of masker intensity (masker and probe frequency are fixed), the probe intensity $I_p(I_m)$ was slowly raised from below-threshold levels until it was just detected by the listeners, at intensity $I_p^*(I_m)$. As before $*$ indicates threshold.

In Fig. 14 f_m = 400 Hz, I_m is the abscissa, f_p is the parameter on each curve, in kHz, and the threshold probe intensity $I_p^*(I_m)$ is the ordinate. The dotted line superimposed on the 3 kHz curve $(I_m/10^{60/10})^{2.4}$ represents the suppression threshold at 60 dB-SL which has a slope of 2.4 dB/dB. The dotted line superimposed on the 0.45 kHz curve has a slope of 1 and a threshold of 16 dB SL.

[10] Fletcher, Wegel, and Lane used the newly invented vacuum tube, developed by Arnold for network transmission, to make these measures [97, 40].

Three regions are clearly evident: the *downward spread* of masking ($f_p < f_m$, dashed curves), *critical band* masking ($f_p \approx f_m$, dashed curve marked 0.45), and the *upward spread* of masking ($f_p > f_m$, solid curves) [98].

Critical band masking has a slope close to 1 dB/dB (the superimposed dotted line has a slope of 1). The downward spread of masking (the dashed lines in Fig. 14) has a low threshold intensity and a variable slope that is less than one dB/dB, and approaches 1 at high masker intensities. The upward spread of masking (USM), shown by the solid curves, has a threshold near 50 dB re sensation level (i.e., 65 dB SPL), and a growth just less than 2.5 dB/dB. The dotted line superimposed on the f_p=3 kHz curve has a slope of 2.4 dB/dB and a threshold of 60 dB.

The dashed box shows that the upward spread of masking of a probe at 1 kHz can be greater than the masking within a critical band (i.e., f_p = 450 Hz $> f_m$=400 Hz). As the masker frequency is increased, this "crossover effect" occurs in a small frequency region (i.e., 1/2 octave) above the masker frequency. The crossover is a result of a well documented nonlinear *response migration,* of the excitation pattern with stimulus intensity, described in a fascinating (and beautifully written) paper by Dennis McFadden [99]. Response migration was also observed by Munson and Gardner in a classic paper on forward masking [100]. This important migration effect is beyond the scope of the present discussion, but is is reviewed in [98, 101], and briefly described in the figure caption of Fig. 27.

The upward spread of masking is important because it is easily measured psychophysically in normal hearing people, is robust, well documented, and characterizes the outer hair cell nonlinearity in a significant way. This psychophysically measured USM has correlates in basilar membrane, hair cell, and neural recording literature, where it is called two–tone suppression (2TS).

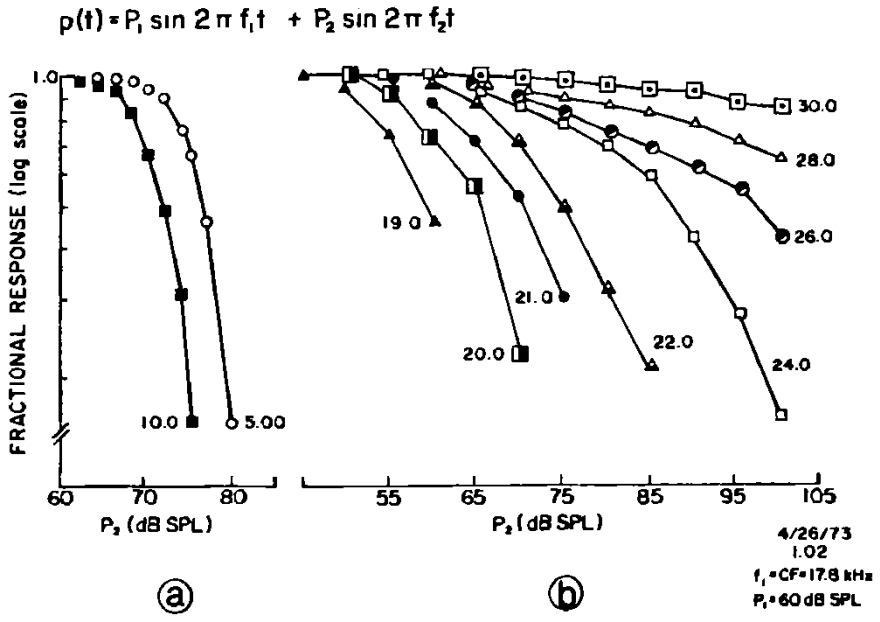

Figure 15: *Two–tone suppression IO functions from Fig. 8 of Abbas and Sachs (1976).*

Two–tone suppression. The neural correlate of the psychophysically measured USM is called *two–tone suppression* (2TS). First a neural tuning curve is first measured. Next a pure tone probe at intensity $I_p(f_p)$, and frequency f_p, is placed a few dB (i.e., 6 to 10) above threshold at the characteristic (best) frequency of the neuron F_{cf} (i.e., $f_p = F_{cf}$). Next the intensity $I_s(f_s)$ of a *suppressor* tone, having frequency f_s, is increased until the rate response to the probe $R(I_p, 0)$ either decreases by a small amount Δ_R, or drops to Δ_R above the spontaneous rate $R(0,0)$. These two criteria are defined

$$R_s(I_p, I_s^*) \equiv R(I_p, 0) - \Delta_R \tag{17}$$

(subscript s for *superthreshold*) and

$$R_t(I_p, I_s^*) \equiv R(0,0) + \Delta_R \tag{18}$$

(subscript t for *threshold*). Δ_R indicates a fixed small but statistically significant constant change in the rate (i.e., Δ_R = 20 spikes/s is a typical value). The threshold suppressor intensity is defined as $I_s^*(f_s)$, and as before the $*$ indicates the threshold suppressor intensity. The two threshold definitions R_s and R_t are very different, and both are useful.

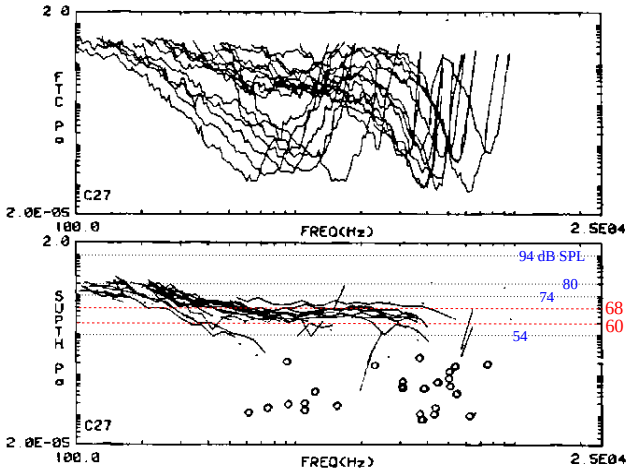

Figure 16: *The upper panel shows a family of neural tuning curves from the cat. The lower panel shows all the 2TS thresholds for this set of tuning curves. The circles are the locations of the F_{cf} bias tone levels and frequencies. The solid lines are the intensity that will cause the suppressed tuning curve tip to be at the same level as that of the bias tone (the circle). The abscissa is in Pascals. 2 Pa is 100 dB SPL. The median suppression threshold at 1 kHz is 0.04 Pa (i.e., 66 dB SPL). For more details see [83].*

Abbas and Sachs' Fig. 8 [86] is reproduced in Fig. 15. For this example, F_{cf} is 17.8 kHz, and the $f_p = F_{cf}$ probe intensity P_1 is 60 dB. This means that the threshold intensity

of the neural tuning curve was a low spontaneous neuron with a relatively high threshold of approximately 50-55 dB SPL. The left panel of Fig. 15 is for apical suppressors that are lower in frequency than the CF probe ($f_s < f_p$). In this case the threshold is just above 65 dB SPL. The suppression effect is relatively strong and independent of frequency. In this example the threshold of the effect is less than 4 dB apart (the maximum shift of the two curves) at suppressor frequencies f_s of 10 and 5 kHz (a one octave seperation).

The right panel shows the case $f_s > f_p$. The suppression threshold is close to the neurons threshold (i.e., 50 dB SPL) for probes at 19 kHz, but increases rapidly with frequency.The strength of the suppression is weak in comparison to the case of the left panel ($f_s < f_p$), as indicated by the slopes of the family of curves.

The importance of the criterion. The data of Fig. 15 uses the first suppression threshold definition Eq. 17 R_s (a small drop from the probe driven rate). In this case the F_{cf} probe is well above its detection threshold at the suppression threshold, since according to definition Eq. 17, the probe is just detectably reduced, and thus audible. With the second suppression threshold definition Eq. 18 R_t, the suppression threshold corresponds to the detection threshold of the probe. Thus Eq. 18, *suppression to the spontaneous rate*, is appropriate for Wegel and Lane's masking data where the probe is at its detection threshold $I_p^*(I_m)$. Suppression threshold definition Eq. 18 was used when taking the 2TS data of Fig. 16, where the suppression threshold was estimated as a function of suppressor frequency.

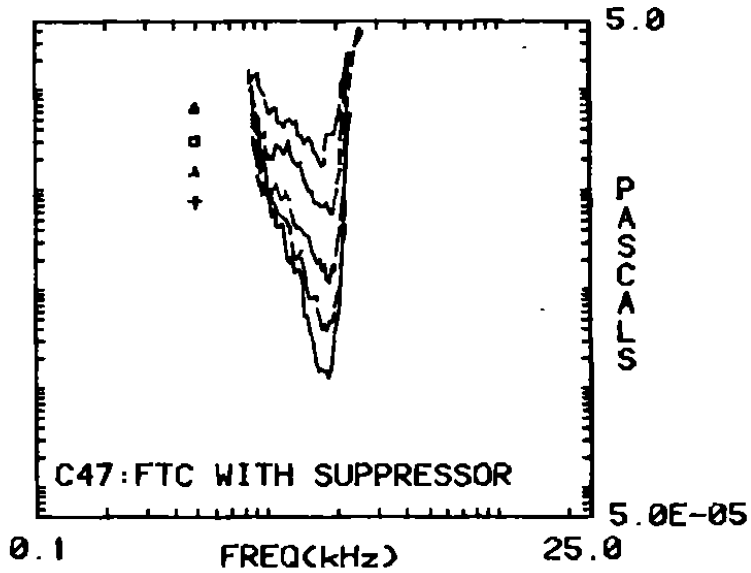

Figure 17: *A cat neural tuning curve taken with various suppressors present, as indicated by the symbols. The tuning curve with the lowest threshold was with no suppressor present. As the suppressor changes by 20 dB, the F_{cf} threshold changes by 36 dB. Thus for a 2 kHz neuron, the slope is 36/20, or 1.8. Interpolation of Fig. 18 gives a value of ≈1.6 dB/dB. One Pascal = 94 dB SPL.*

To be consistent with a detection threshold criterion, such as the detection criterion used in by Wegel and Lane in psychophysical masking, (Eq. 18) must be used. To have a tuning

curve pass through the F_{cf} probe intensity of a 2TS experiment (i.e., be at threshold levels), it is necessary to use the suppression to rate criterion given by Eq. 18. This is shown in Fig. 17 where a family of tuning curves is taken with different suppressors present. As described by Fahey and Allen (1985), when a probe is placed on a specific tuning curve of Fig. 17, corresponding to one of the suppressor level symbols of Fig. 17, and a suppression threshold is measured as shown in Fig. 16 (lower panel), that suppression curve will fall on the corresponding suppression symbol of Fig. 17. There is a symmetry between the tuning curve measured in the presents of a suppressor, and a suppression threshold obtained with a given probe. This symmetry only holds for criterion Eq. 18, the detection threshold criterion, which is appropriate for Wegel and Lane's data.

Suppression threshold. Using the criterion Eq. 18, Fahey and Allen (1985) showed (Fig. 16) that the suppression threshold $I_s^*(I_p)$ in the tails is near 65 dB SPL (0.04 Pa). This is true for suppressors between 0.6 and 4 kHz. A small amount of data are consistent with the threshold being constant to much higher frequencies, but the Fahey and Allen data are insufficient on that point.

Arthur *et al.* (1971), using Eq. 17, reported that when $f_s > f_p$ the suppression threshold was *more* sensitive than the CF threshold. Fahey and Allen [83] used Eq. 18, and found *no* suppression for $f_s > f_p$, except for very high threshold neurons. This is because the rate never was suppressed to threshold for high frequency suppressors. For high frequency suppressors ($f_s > f_p$), suppression is a weak effect so it cannot suppress to threshold (Eq. 18) unless the neurons threshold is very high (greater than 60 dB SPL). This means that suppression above CF ($f_s > f_p = F_{cf}$) can only be observed for low spontaneous, high threshold neurons, when using Eq. 17.

Suppression slope. Bertrand Delgutte has written several insightful papers on masking and suppression [103, 102, 104]. As shown in Fig. 18, he estimated how the intensity growth slope (the ordinate, in dB/dB) of 2TS varies with suppressor frequency (the abscissa) for several probe frequencies (the parameter indicated by the vertical bar) [102]. As may be seen in the figure, the suppression growth slope for the case of a low frequency apical suppressors on a high frequency basal neuron (the case of the left panel of Fig. 15), is ≈2.4 dB/dB. This is the same slope as Wegel and Lane's 400 Hz masker, 3 kHz probe USM data shown in Fig. 14. For suppressor frequencies greater than the probe's ($f_s > f_p$), Delgutte reports a slope that is significantly less than 1 dB/dB. Likewise Wegel and Lane's data has slopes much less than 1 for the downward spread of masking.

Related data. Kemp and Chum [105] (their Figs. 7 and 9) found similar suppression slopes of more than 2 dB/dB for low frequency suppressors of *Stimulus frequency emissions* (SFE). This data seems similar to the USM and 2TS data, but is measured objectively from the ear canal. New data on the suppression slope has been recently published by Pang and Guinan (1997).

In Fig. 19 Liberman and Dodds show the complex relationship between the state of the inner hair cell tuning and outer hair cell damage [43]. Local noise trauma to the outer hair cell produces tuning curves with *elevated tips* and *increased sensitivity* in the low frequency tails. There is a notch near F_z.

The development work of Walsh and McGee [106] shows similar results, with hyper sensitive tails and W shaped tuning.

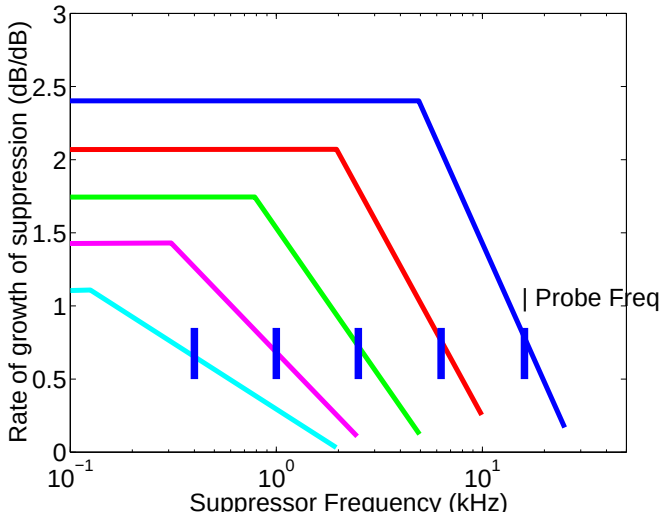

Figure 18: *This family of curves, redrawn from Delgutte (1990b), describes the growth of suppression, in dB/dB, as a function of the frequency of the suppressor (the abscissa, in kHz). The frequency of the probe tone is the parameter, as indicated by the heavy vertical line. For example, this figure shows that for neurons having a best frequency of 15 kHz, the maximum 2TS slope is ≈2.4 dB/dB and occurs for suppressors between 100 and 5 kHz. A neuron having a 1 kHz best frequency has a maximum 2TS slope of ≈1.4 dB/dB for suppressors between 100 and 300 Hz. When the suppressor frequency approaches the excitatory region of the neuron, the suppression slope is not measurable, since the suppressor drives the neuron in this case, making the rate suppression unmeasurable. Suppression above the probe frequency is a very weak effect because the slope is much less than 1.*

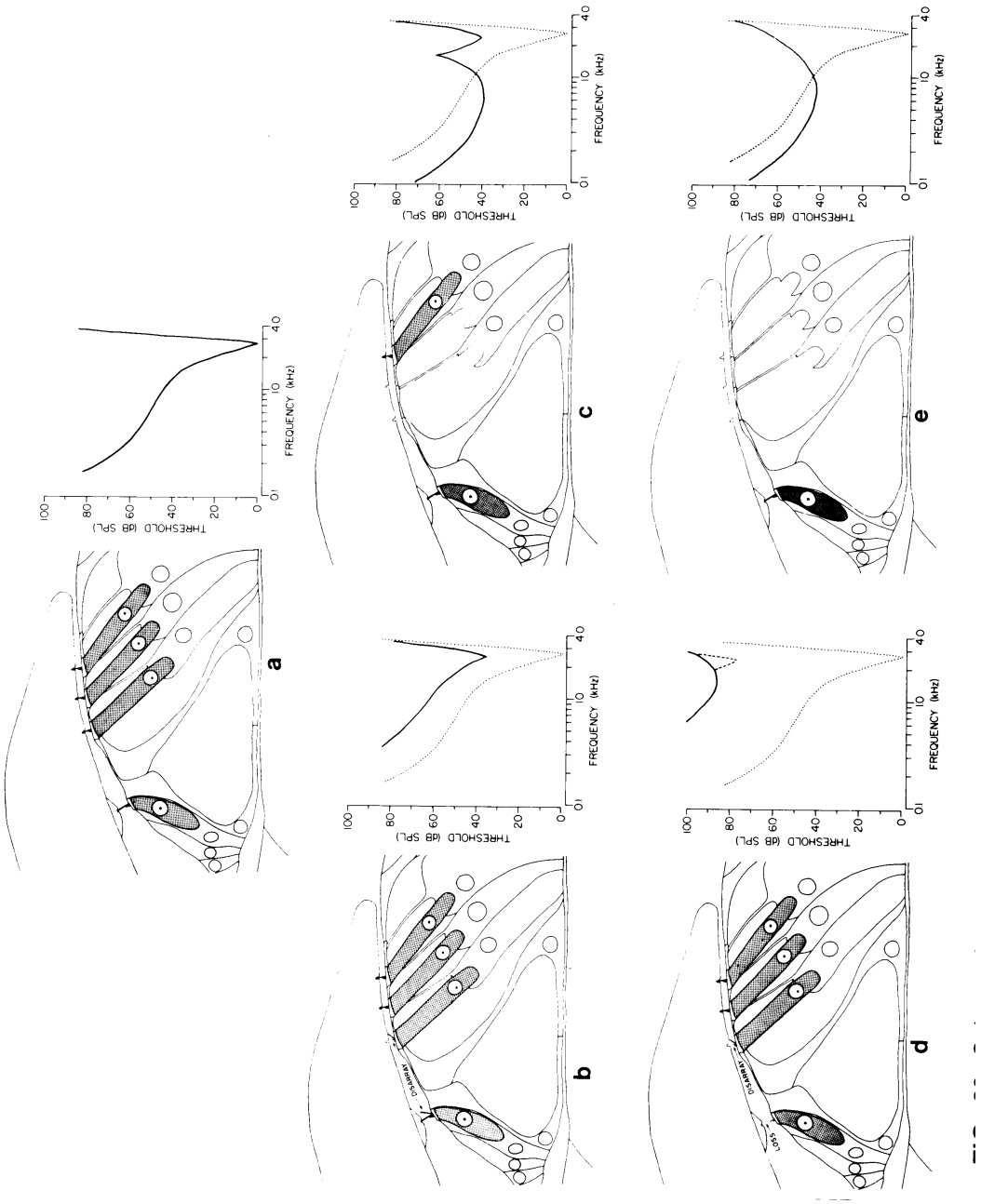

Figure 19: *Figure from Liberman and Dodds showing the effect of OHC damage on neural responses [43]. These classic studies are hard to explain with the cochlear amplifier concept.*

It is widely recognized that both the Liberman and Dodds as well as the Walsh and McGee [106] studies give us an important insight into micromechanics, but nobody has a simple explanation of exactly what these results mean. One likely possibility is that there are higher order modes (i.e., degrees of freedom) within the organ of Corti and the tectorial membrane.

Summary. The USM and 2TS data show systematic and quantitative correlations between the threshold levels and slopes. The significance of this correlation has special importance because (a) it comes from two very different measurement methods, and (b) Wegel and Lane's USM and Kemp's SFE data are from human, while the 2TS data are from cat, yet they show quite similar responses. This implies that the cat and human cochleae may be quite similar in their nonlinear responses.

The USM and 2TS threshold and growth slope (e.g., 50 dB-SL and 2.4 dB/dB) are important features that must be modeled before we can claim to understand cochlear function. While there have been several models of 2TS [107, 64, 108] as discussed in some detail by Delgutte [102], none are in quantitative agreement with the data. The two–tone suppression model of Hall [64] is an interesting contribution to this problem because it qualitatively explores many of the key issues.

2.2.6 The basilar membrane to hair cell transformation

The purpose of this section is to address the two intertwined problems mentioned in Sec. 2.1.1, *cochlear frequency selectivity* and *cochlear nonlinearity*,

A key question is the nature of the transformation between BM and hair cell cilia motion at a given location along the basilar membrane. There are several issues here. First, the motion of IHC and OHC cilia are not the same. The IHC cilia are believed to be free standing while the tips of OHC cilia are firmly anchored in the underside of the tectorial membrane. We may avoid this uncertainty by changing the question: *What is the transformation between BM and TM-RL shear?* (Basilar membrane (BM), tectorial membrane (TM) and reticular membrane (RL). The IHC and OHC cilia sit in the space between TM and RL.) The cilia sit in a 4-6 μ m fluid filled space between the tectorial membrane and the rectular lamina. It is the shearing motion between these two surfaces that moves the inner and outer hair cell cilia. The question reduces to the nature of the coupling between the vertical displacement of the BM and the radial shear of the TM-RL space. We dichotomize the possibilities into *single* versus *multi-mode* coupling. It is presently a matter of opinion as to which of these two couplings accounts for the most data.

Single-mode coupling. One possibility is that the displacement of the basilar membrane is functionally the same as the displacement of the TM-RL shear (and implicitly therefore the same as the OHC cilia). I will call this model *single-mode coupling* between the basilar membrane and the TM-RL shear. This means that the displacement magnitude and phase of these two displacements are significantly different. For example, they might differ by a linear transformation.

Since about 1971 when Rhode published Fig. 10, the *single-mode coupling* view has become widely accepted [2, 92, 109, 110]. This is unfortunate since it is *not* generally true that experimental BM displacement, IHC voltage frequency response, and neural tuning curves are identical, or even similar. Nobody has actually demonstrated that neural and

basilar membrane responses are functionally the same. The strongest argument for single-mode coupling is the study of [92] which is at one frequency and in one species. Even this data shows a small, systematic and unexplained 3.8 dB/oct difference across frequency.

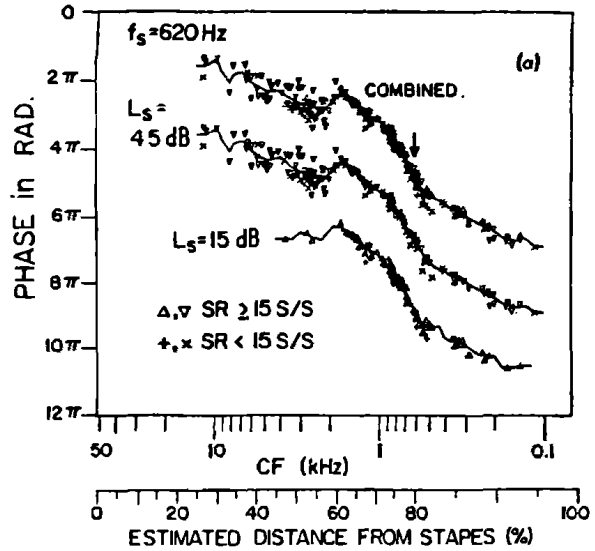

Figure 20: *Figure from Kim et al. 1979. The arrow indicates the frequency of the tone. The abscissa is the F_{cf} of each neuron, and the ordinate is the neural phase of the neuron relative to the phase in the ear canal. Like the data of Fig. 19, this figure shows evidence for* multi-mode coupling *between the BM response and the cilia excitation.*

Multi-mode coupling. The alternative to single-mode coupling is that neural signals are a multi-mode mechanics transformation of the basilar membrane response.[11] There are many studies that are in conflict with single-mode coupling. There are at least two categories of measurements that give insight into this transformation, *tuning* and *nonlinearity*. The following discussion summarizes many of the known differences between basilar membrane and neural response.

Noise damage. In my view Fig. 19 gives strong direct evidence of a tectorial membrane resonance (multi-mode "2 degrees of freedom" coupling). But this view has remained controversial. One problem with these data is the difficulty in interpreting them. But no matter what the interpretation, the data of Fig. 19 do not seem compatible with the concept of single-mode coupling.

Neural phase populations. As discussed extensively by this author on many occasions, phase measurements of the mechanical response and the neural response are fundamentally incompatible. Basilar membrane data has a monotonically lagging phase. Neural data

[11]The multi-mode transformation could even be nonlinear if OHCs are involved. For now we shall stick to linear multi-mode transformations.

shows a 180 degree phase reversal at F_z (see Fig. 9), where the tip and tail meet in the tuning curve, as shown at the 60% location along the basilar membrane (2 kHz place) in Fig. 20. The implication of this is that there is a well defined antiresonance (transmission zero) in the neural response at the frequency, where the tip and tail meet, that does not exist in the basilar membrane data.

Tuning curve S_2 slopes. Another line of reasoning comes from the cat neural tuning curve S_2 slopes as seen in Tab. 1 and Figs. 12 and 16 for high frequency neurons. Slope S_2 for cat neural tuning curves having F_{cf}'s greater than 3 kHz are typically greater than 50 dB/oct. From Fig. 13, typical cat tuning curves in the 15 kHz range have S_2 slopes greater than 100 dB/oct [90]. The slope S_1 of the basilar membrane response of Fig. 11 is 10 dB. If we make a middle ear correction of -10 dB/oct (this is equivalent to a normalization with respect to ear canal pressure rather than incus displacement), the S_2 slope of Fig. 11 would be S_2' = S_2-10 = 30-10 = 20 dB/oct.

Tuning curve "tails." Neural tuning curve "tails" of high frequency neurons typically have threshold levels in excess of 65 dB SPL, as may be seen in Fig. 12 and Fig. 16.[12] The S_1 slopes of neural responses in the tail are close to zero. Basilar membrane tuning curves do not have such tails.

BM versus neural 2TS. Recent basilar membrane 2TS measurements [111, 112, 108] have unequivocally shown that the neural and BM 2TS thresholds are significantly different. For example, Ruggero *et al.* (page 1096) says

> . . . if neural rate threshold actually corresponds to a constant displacement ($\approx$ 2 nm) . . . , then mechanical suppression thresholds would substantially exceed neural excitation thresholds and would stand in disagreement with findings on neural rate suppression.

Using a 0.1 nm displacement criterion, Cooper found basal excitation thresholds near 65 dB and 2TS thresholds near 85 dB SPL. Cooper says (page 3095, column 2, mid-paragraph 2)

> Indeed, the direct comparisons shown . . . indicate that most of the low-frequency mechanical suppression thresholds were between 10 and 20 dB above the iso-displacement tuning curves . . . [corresponding] to "neural thresholds" at the site's [CF].

That is, Cooper's BM results placed the threshold of BM suppression about 1 order of magnitude higher in level than the Fahey and Allen 2TS thresholds shown in Fig. 16, both in absolute terms, and relative to the 0.1 nm threshold. The Geisler and Nuttall (1997) study [108] confirms these findings (see their Fig. 2).

BM versus other bandwidth estimates. BM displacement response are not in agreement with psychoacoustic detection experiments of tones in wide band noise, such as the *critical ratio* experiments of Fletcher [36, 113], French and Steinberg [114], and Hawkins

[12] Because of the reversed ordinate scale of Fig. 12, the tails lie below 65 dB in this figure.

and Stevens [115]. These classic studies show that the psychoacoustic bandwidth is nearly independent of intensity over more than a 55 dB range. Neural revcore functions also show that the bandwidth is independent of level from threshold to 50 dB-SL[116] (see Fig. 6). The bandwidths of the basilar membrane data, on the other hand, are quite variable, as may be inferred from Figs. 10 and 11.

BM Model predictions. When the 2^d and 3^d models began showing sharpened responses relative to the transmission line model, the hope was that these more detailed models would converge to the response measured in the nerve fiber. Although a significant increase in sharpness was found, the necessary convergence has *not* occurred. From a theoretical point of view, it is significant that the frequency response, as computed by passive cochlear models of basilar membrane motion, is quite different from the response estimated from the nerve fiber measurements. The difference (i.e., the error) in excess gain, as defined in Fig. 9, is somewhere between 10 to 100 (20 to 40 dB).

2.2.7 Measures from the ear canal

Acoustic Distortion products It has been known for over a century that the ear generates distortion in response to pairs of tones. Helmholtz believed that this distortion came from the middle ear. Now we now know that this distortion is a byproduct of normal outer hair cells. In the last 15 years commercial equipment has been developed to detect hearing loss in infants based on these distortion product emissions. Using *combination tones*, such as the $2f_1 - f_2$ distortion product, Goldstein was one of the first to emphasize the importance of nonlinearity in hearing at low intensities [60, 61]. Ever since Goldstein's 1967 classic study, distortion product analysis has have been an important experimental tool, which has helped us to understand the inner ear. Distortion products are a byproduct of outer hair cell dynamic range compression, but otherwise do not directly play any know role in hearing. Smoorenburg [62] was the first to observe that the distortion product disappeared in those hears having a hearing loss. By the use of the cochlear microphonic, Deatherage *et al.* [117] and much later Kim [82] demonstrated that the distortion products are present on the basilar membrane by showing that these nonlinear tones propagated along the basilar membrane. Then in 1978 Kemp directly observed the distortion product in the ear canal, leading to much of the OAE diagnostic equipment presently used in infant screening [75].

Ear canal standing waves. In 1958 Elliott [120] observed the fact that the threshold of hearing is not a smooth function of frequency but fluctuates in a quasi-periodic manner with a period of $\approx$80-100 hertz near 1200 Hz. Such micro-structure is characteristic of standing waves due to an impedance mismatch within the basilar membrane [75, 118, 119].

Starting in 1978, Kemp [56, 74, 75] observed low level dispersive ear canal pressure responses (he called them *echos*) to a pulse of sound in the ear canal. The delays approximately correspond to a round trip travel time along the basilar membrane. These "echos" displayed nonlinear compressive growth with intensity.

A third somewhat bizarre observation followed with the finding of *spontaneous otoacoustic emissions* (SOAEs), which are narrow band tones emanating from the human cochlea [75, 121]. It is natural to relate Elliott's micro-structured hearing threshold and Zwicker and Schloth's super-threshold ear canal pressure microstructure [118, 119] to

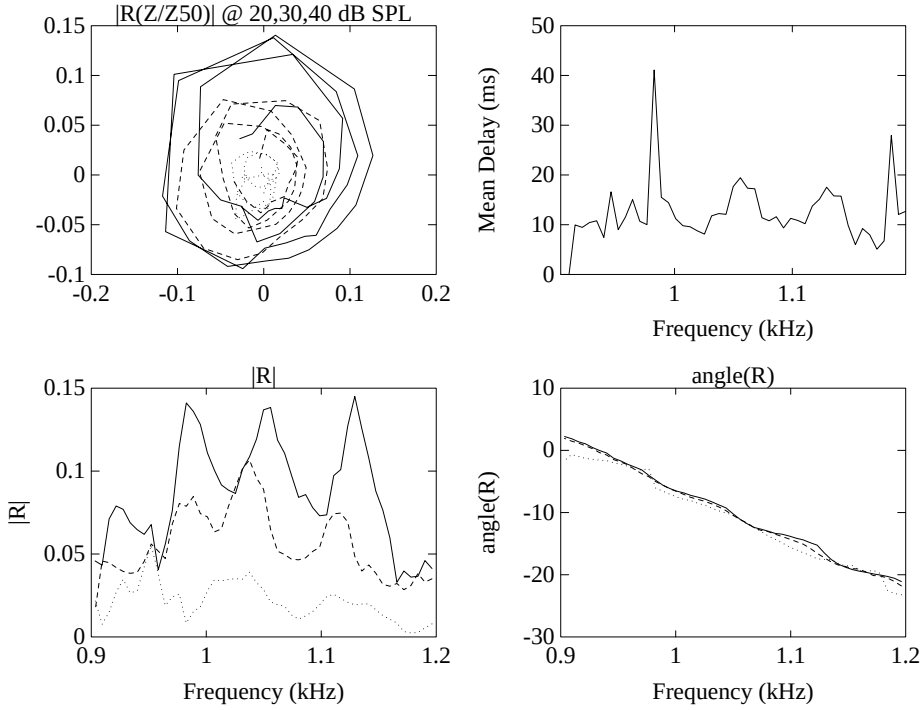

Figure 21: *Kemp [75, 105] and later Zwicker and Schloth [118] reported that the pressure in the ear canal is level dependent. In 1995 Allen, Shaw, and Kimberley measured the nonlinear ear canal impedance in normal ears below 50 dB SPL [119]. They found that the ear canal effects of pressure, reflectance, impedance, spontaneous emissions, hearing thresholds, and distortion products, had the same microstructure. Some of this data are shown in Fig. 22. It seems clear that the organ of Corti impedance changes with level are due to outer hair cell dependence. The upper–left panel of this figure shows a polar plot of the pressure reflectance at three different sound levels. The radius gives the magnitude and the angle the phase of the complex reflectance. The lower–left panel shows the magnitude of the ratio of the retrograde to incident pure tone pressure $|R|$ for pure tones of 20, 30, and 40 dB SPL (the power ratio is $|R|^2$). The panels on the right show the group delay (upper) and phase (lower) of the pressure reflectance. The raw data for this plot was provided by Greg Shaw and Barry Kimberley of the University of Calgary.*

these narrow band SOAE tones. In animals, similar tones have been correlated with damage to the cochlea, where a clear discontinuity in cochlear impedance is likely.

The first speculation was that these emissions were just biological noise, passively amplified by cochlear standing waves [75]. However, linearly filtered noise must have a Gaussian amplitude distribution. Contrary to the standing wave model, the amplitude distribution of the emissions were more like tones [122].

In a transmission line, the reflectance of energy is determined by the ratio of the load impedance at a given point, divided by the local characteristic impedance of the line. Following up on these ideas, as shown in Fig. 21, Allen *et al.* [119] measured the canal impedance at 20, 30, 40, and 50 dB SPL, and used the 50 dB SPL ear canal impedance as a Thévenin cochlear source impedance. This allowed them to estimate the nonlinear component of the retrograde power below 50 dB SPL. From Fig. 21 we see that the reflectance is stimulus–level dependent. The nonlinear canal power reflectance covaries with the nonlinear compression characteristics seen by the inner hair cells (IHC), which are measured psychophysically in terms of compressive loudness growth. Lower stimulus intensities lead to larger reflections from the basilar membrane. This data leads to the conclusion that the relative local impedance is stimulus–level dependent.

Based on the ear canal impedance measurements shown in Figs. 21 and 22, and given what we know about OHC properties, the most likely cause of nonlinear basilar membrane impedance changes with level would be due to changes in the OHC stiffness. This conclusion logically follows from ear canal impedance measurements expressed as the nonlinear power reflectance, defined as the retrograde to incident power ratio [119].

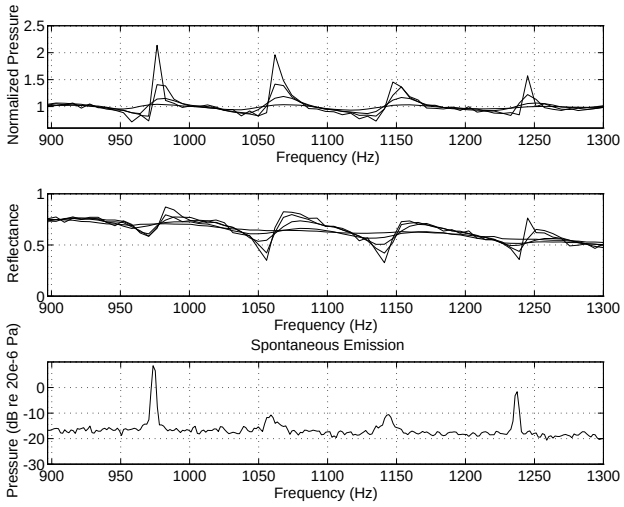

Figure 22: *Pressure, pressure reflectance, and the ear canal pressure power spectrum noise floor showing SOAE. There is a nearly perfect correlation across frequency between these three measures, as well as the threshold of hearing microstructure. All of the measure are consistent with very low damping standing waves, and a model of the cochlea that has very low losses [119].*

A model that seems to account for the data of Figs. 21 and 22 is Kemp's standing wave model [75, 76], but modified to include a nonlinear load impedance, as shown in Fig. 23. It is imagined that this termination impedance is distributed along the length of the basilar membrane. Only one location is shown in Fig. 23.

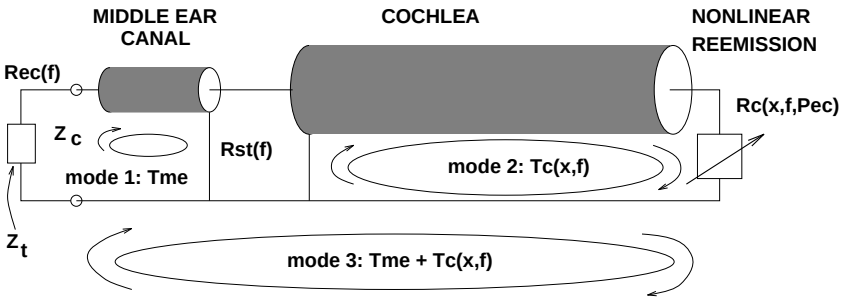

Figure 23: *A simple model of the cochlea that accounts for the 1995 observations of Allen, Shaw and Kimberley [119].*

Can the nonlinear model of Fig. 23 fix this amplitude distribution, and save Kemp's standing wave model? To investigate the feasibility of this model, an extension of Elliott, Kemp, and Zwicker's observations are shown in Fig. 22 [119]. In this figure the ear canal pressure, the pressure reflectance and impedance, and the spectral noise floor all show microstructure. The nonlinear element accounts for the level dependent reflectance of Fig. 21 low left panel, as well as the standing waves and other data of Fig. 22. This model assumed that thermal noise drives the standing waves to give spontaneous emissions (bottom panel of Fig. 22).

2.2.8 Loudness growth, recruitment and the OHC

In 1924 Fletcher and Steinberg published an important paper on the measurement of the loudness of speech signals [123]. In this paper, when describing the growth of loudness, the authors state

> the use of the above formula involved a *summation of the cube root of the energy rather than the energy*.

This cube–root dependence had first been described by Fletcher the year before [16].

In 1930 Fletcher postulated that there was a monotonic relationship between central nerve firings rates and loudness. Given a tonal stimulus at the ear drum, Stevens' law says that the loudness is given by

$$L \equiv L(f, x, I) \propto I^{\nu}, \tag{19}$$

where $\{f, x, I\}$ are the frequency, place and intensity of the tone, respectively. The exponent ν has been experimentally established to be in the range between $1/4$ and $1/3$ for long duration pure tones at 1 kHz. Fletcher and Munson (1933) found $\nu \approx 1/4$ at high intensities and approximately 1 near threshold. Although apparently it has not been adequately documented, ν seems to be close to 1 for the *recruiting ear* [124].

Recruitment. What is the source of Fletcher's cube root loudness growth (i.e., Stevens' Law)? Today we know that cochlear outer hair cells (OHC) are the source of the cube root loudness growth observed by Fletcher.

From noise trauma experiments on animals and humans, we may conclude that recruitment (abnormal loudness growth) occurs in the cochlea [125, 126]. Steinberg and Gardner (1937) described such a loss as a "variable loss" (i.e., sensory–neural loss) and

partial recruitment as a mixed loss (i.e., having a conductive component) [8, 127]. They and Fowler verified the conductive component by estimating the air–bone gap. In a comment to Fowler's original presentation on loudness recruitment in 1937, the famous anatomist Lorente de No theorized that recruitment is due to hair cell damage [7]. Steinberg and Gardner clearly understood recruitment, as is indicated in the following quote [8, page 20]

> Owing to the expanding action of this type of loss it would be necessary to introduce a corresponding compression in the amplifier in order to produce the same amplification at all levels.

This compression/loss model of hearing and hearing loss, along with the loudness models of Fletcher [128], are basic to an eventual quantitative understanding of nonlinear cochlear signal processing and the cochlea's role in detection, masking and loudness in normal and impaired ears. The work by [129] and [8], and work on modeling hearing loss and recruitment [130] support this view.

In summary, many studies agree: The cube–root loudness growth starts with the nonlinear compression of basilar membrane motion due to stimulus dependent voltage changes within the OHC.

2.3 Discussion

When spontaneous emissions were first observed, many researchers were quick to conjecture that the cochlea was an "active system," which occasionally became unstable [75, 118, 131], hence models that incorporate negative damping were proposed [94, 132, 133, 109, 110, 134]. The use of negative damping in these models serves the function of sharpening the tuning of the cochlear filters. It also has the capability, in theory, of making the basilar membrane oscillate, thus giving rise to the emissions that were observed by Kemp.

While this seems like an attractive approach, one problem has been finding a model that is physically realizable. In my view, negative resistance is too radical. It is not a good theoretical solution because it could introduce instability that would be much worse than a few tones in the ear canal. For example, it would mean that waves traveling in either direction would be amplified. This would create total havoc, and is inconsistent with observations of wave amplitudes seen in the canal, which are consistent with very low loss traveling waves [135]. Negative damping was introduced to improve cochlear frequency selectivity and sensitivity. I believe we need to find different solutions to these two problems.

So far the *motile hair cell* model has not been a particularly successful concept. There have been a host of problems. One of the most difficult is the role of the OHC membrane capacitance, which acts as a low pass filter on the cell membrane voltage. Due to this filtering effect, the magnitude of the motion becomes small just where the boost in gain is needed, at high frequencies. A second problem has been the phase of the motility, which is reversed from the preferred direction. Time delay has been used in an attempt to fix this difficulty.

Are the many differences between basilar membrane and neural (i.e., TM-RL shear) significant, or are they an artifact of the experimental technique? Unfortunately, we cannot yet be sure of the answer to this important question.

It is widely recognized that key nonlinear properties are missing from modern cochlear models. The question is, *What is the modification that needs to be made to the models to extend them?* This question will be discussed in Sec. 4. However until the experimental questions are resolved, it seems that this theoretical question is likely to remain open.

3 Outer Hair Cell Transduction

The fundamental question in cochlear research today is:

What is the role of the outer hair cell (OHC) in cochlear mechanics?

3.1 Role of the OHC

The prevailing view is that the OHC provides *cochlear sensitivity* and *frequency selectivity* [2, 92, 109, 110].

The alternative view, argued here, is that the OHC compresses the excitation to the inner hair cell, thereby providing dynamic range expansion.

There is an important (and possibly subtle) difference between these two views. The first view deemphasizes the role of the OHC in providing dynamic range control (the OHC's role is to improve sensitivity and selectivity), and assumes that the nonlinear effects result from OHC saturation. The second view places the dynamic range problem as the top priority. It assumes that the sole purpose of the OHC nonlinearity is to provide dynamic range compression, and that the OHC plays no role in either sensitivity or selectivity, which are treated as independent issues.

3.1.1 The dynamic range problem

The question of how the large 120 dB dynamic range of the auditory system is attained has been a long standing problem. Previously this question has been raised in the context of both the nerve cell, and the synapse. I am raising the same question, but presynaptically.

Our understanding of the auditory system's large 120 dB dynamic range is fundamentally incomplete. For example, *recruitment*, the most common symptom of neurosensory hearing loss, is best characterized as the loss of dynamic range [8, 136, 40, 124]. Recruitment results from outer hair cell damage [125]. To successfully design hearing aids that deal with the problem of recruitment, we need models that improve our understanding of *how* the cochlea achieves its 120 dB dynamic range.

Based on a simple analysis of the IHC voltage, we will show that the dynamic range of the IHC must be less than 65 dB. In practice it is widely accepted that IHC dynamic range is less than 50 dB.

The IHC's transmembrane voltage is limited at the high end by the cell's open circuit (unloaded) membrane voltage, and at the low end by thermal noise. There are two obvious sources of thermal noise, cilia Brownian motion, and Johnson (shot) noise across the cell membrane (Fig. 24).

The obvious question arises: *How can the basic cochlear detectors (the IHCs) have a dynamic range of less than 65 dB, and yet the auditory system has a dynamic range of 120 dB?* The huge amount of indirect evidence has shown that this increased dynamic range results from mechanical nonlinear signal compression provided by outer hair cells. This dynamic range compression shows up in auditory psychophysics and in cochlear physiology in many ways.

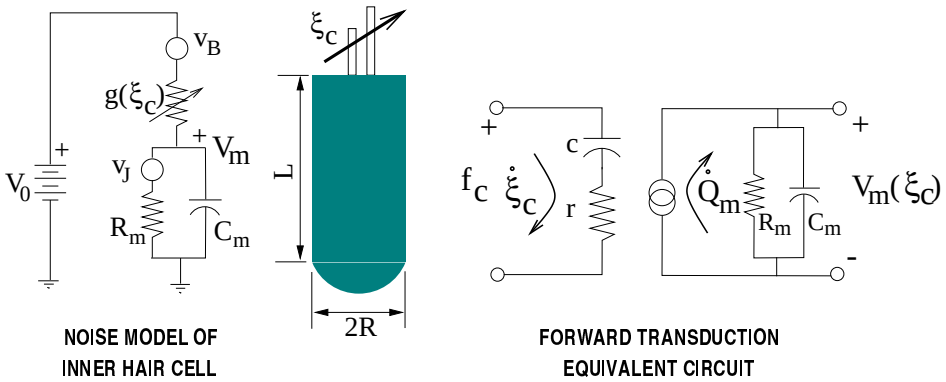

Figure 24: *On the left is the equivalent circuit model of a hair cell with noise sources due to the cell leakage resistance Johnson noise v_J and the Brownian motion of the cilia, represented by the voltage noise source v_B. On the extreme right is the linearized small–signal equivalent circuit, which may be used to find the $ABCD$ transmission parameters described by Eq. 21. The force on the cilia f_c and the cilia velocity ξ_c are related by the cilia drag r and drag compliance c. The voltage in the cell V_m depends on the membrane electrical admittance $1/R_m + sC_m$ and the cilia induced current $\dot{Q}_m$. The left-hand electrical circuit Eq. 22 determines this relationship.*

IHC dynamic range. From the model described by Fig. 24 the mean-squared transmembrane thermal (Johnson) noise voltage v_J of the IHC is given by

$$v_J^2 = 2kTR_m \int_{-\infty}^{\infty} \frac{1}{1 + (2\pi f R_m C_m)^2} df = \frac{kT}{C_m}, \tag{20}$$

where R_m is the membrane leakage resistance and C_m the membrane capacitance [137, 78]. The IHC capacitance has been found to be about 9.6 pF by Kros and Crawford [138]. From Eq. 20, v_J = 21.1 μV RMS at body temperature (k = 1.38$\times$10^{-23} Joule/degree-Kelvin, T = 310° K).

The maximum open circuit DC voltage across the cilia is about 120 mV. The RMS voltage corresponding to a peak to peak voltage of 120 mV is $(120/2)/\sqrt{2} = 42$ mV. The maximum RMS cell voltage that has been empirically observed is 30 mV RMS (Russell, personal communication). The ratio of 30 mV RMS to the noise floor voltage (e.g., 21.1 μV RMS), expressed in dB, is 63 dB.

It has been shown by Denk [139] that the Brownian motion of the cilia (thermal noise motion) is larger than the Johnson noise. Since it is difficult to calculate the soma voltage change due to Brownian motion, we first calculate the Johnson noise. A correction can then be made to the Johnson noise based on Denk's observation, to obtain the final estimate of the IHC dynamic range. If we subtract 6 dB from the above estimate of 63 dB, find a reasonable upper limit of 57 dB. The maximum dynamic range in signal intensity of the auditory system is less than 120 dB. This leaves up to 63 dB of dynamic range unexplained.

We conclude that *there must be nonlinear compression (level dependent gain) built into the mechanics of the cochlea* to account for the large acoustic dynamic range. Since the discovery of loudness recruitment in 1937, it has been suspected that OHCs provide this dynamic range compression [7, 8, 125].

The key question before us is: *What is the chain of events that leads to the stimulus compression seen by the IHCs?*

3.1.2 The IHC sensitivity

Russell *et al.* (1986) have estimated the *in vitro* sensitivity of the mouse culture hair cell as 30 mV/degree (0.4 mV/nm) of angular rotation of stereo cilia. Since the maximum observed RMS voltage is 30 mV, 1 degree of cilia displacement is approximately the maximum cilia angular displacement, assuming a linear relationship. This means that an angular displacement of more than a degree, corresponding to a cilia tip displacement of 30/0.4 = 75 nm, would drive the cell into nonlinear saturation. Displacements greater than 75 nm therefore would likely rupture the delicate structures of the cilia transduction channels and tip links. Assuming a thermal noise floor of 20 μV RMS and 30 mV/degree, the IHC displacement sensitivity of the cell at the thermal noise threshold is 0.05 nm. This is about 1/2 the diameter of the hydrogen atom (0.1 nm), and is much smaller than the numbers assumed in many of the basilar membrane measurements for the "iso-response" threshold. This number probably somewhat underestimates the threshold because it ignores the Brownian motion of the cilia. It is difficult to make this correction, but it is likely to be less than a factor of 3 (i.e., 10 dB). More information is needed to refine these estimates.

By way of comparison, the accepted maximum displacement of the stapes at 120 dB SPL is about 1 μm (1000 nm) of displacement [141]. This leads to a corresponding stapes displacement at 0 dB SPL of about 0.001 nm. At 14 dB SPL, which is the typical threshold pressure at the ear drum, the stapes displacement would be 0.005 nm, which is 10 times (20 dB) smaller than the cilia thermal noise threshold displacement estimate of 0.05 nm derived from the 30 mV/degree sensitivity estimate of Russell *et al.* [140]. To match the stapes displacement at threshold to the cilia displacement at threshold would require a linear and passive cochlear gain of 10 (20 dB), which is typical of both models and basilar membrane data. For example in Fig. 10 the high level gain is close to 15 dB, while in Fig. 11 it approaches 40 dB.

The calculated threshold value of 0.05 *nm*, based on Russell's 30 mV/degree estimate, is much smaller than the sensitivities assumed by those making basilar membrane measurements [55, 111, 112, 108]. If the IHC is much more sensitive than previously estimated, then the need for a cochlear amplifier gain is directly reduced by that amount.

3.2 Outer Hair Cell Motility model

A most significant finding in 1985 was of OHC *motility*, namely that the OHC changes its length by up to 5% in response to the cell's membrane voltage [57, 142, 143]. This observation led to a huge increases in research on the OHC cell's motor properties.

In 1999 it was shown that the cell's longitudinal soma stiffness changes by at least a factor of 2 ($>$100%), again as a function of cell membrane voltage [79, 80]. A displacement of the cilia in the direction of the tallest cilia, which is called a *depolarizing* stimulus, decreases the magnitude of the membrane voltage $|V_m|$, *decreases* the longitudinal soma stiffness, and *decreases* the cell soma length. A hyper polarizing stimulus increases the stiffness and extends the longitudinal soma length.

Given this much larger relative change in stiffness (a factor of 2) compared to the relative change in length (a factor of 1.05), for a maximum voltage change, it seems possible that the observed length changes (the motility) is simply a result of the voltage dependent stiffness. For example, imagine a spring stretched by applying a constant force (say a weight), and then suppose that the spring's stiffness decreases. It follows from Hooke's Law (Eq. 4) that the spring's length will *increases* when the stiffness decreases.

Each cell is stretched by its internal "turgor pressure" $\mathcal{P}$ [144], and its stiffness is voltage controlled [79, 80]. The voltage dependent relative stiffness change is a much greater than the relative motility change. Thus we have the necessary conditions for a stiffness induced motility. The consequences of this senerio could be quite significant as there would be no need for an "area" motor [145], defined as the active change in the membrane area with membrane voltage. Many of the nonlinear cochlear models are based on such motility (voltage dependent OHC movement) in a feedback loop.

A voltage dependent stiffness (i.e., a "stiffness motor" [145]) in a feedback loop is a very different model, with some interesting properties. For example, nonlinear resistance models, the first form of cochlear model nonlinearity, represent a voltage dependent impedance mechanism. But they proved insufficient to account for the data [110]. It is possible of course that *both* nonlinear stiffness and resistance are inextricably linked, due to internal mechanisms. But that would be significantly more complex. Simplicity requires that just one mechanism account for the data. The possibility therefore, that the voltage dependent stiffness is the only mechanism, needs careful consideration.

However there seems to be a problem. A decrease in a springs stiffness leads to an *increased* length. Paradoxically, this is the reverse of what OHC soma does, since depolarization gives a decrease in stiffness, and a *shortening* of the soma. In fact there may be no contradiction, if we treat the membrane as having a thickness and composed of a homogeneous iso-volume structure having a Poisson ratio of 1/2. A model is required to sort this out [144, 146].

3.2.1 Equations of the OHC transducer.

Using the methodology described around Eq. 6, the small–signal response of the hair cell transduction may be full described.

Forward transduction In the case of the outer hair cell forward transduction, the input variables are the cilia force (effort) f_c and velocity (flow) $\dot{\xi}_c$.[13] The output variables are the membrane voltage (effort) V_m and current (flow) $\dot{Q}_m$, represented here as the time rate of change of the membrane charge. Assuming linearity, the membrane voltage and current are related by the *membrane admittance* $Y_m(s) = 1/R_m + sC_m$ (admittance $\equiv$ 1/impedance), which is nonlinear (C_m is voltage and/or charge dependent). For this case Eq. 6 is

$$\begin{bmatrix} V_m \\ \dot{Q}_m \end{bmatrix} = \begin{pmatrix} A_f & B_f \\ C_f & D_f \end{pmatrix} \begin{bmatrix} f_c \\ \dot{\xi}_c \end{bmatrix}. \tag{21}$$

This equation may be used to represent the circuit diagram shown in the right side of Fig. 24, thereby specifying the four functions $A_f(s)$, $B_f(s)$, $C_f(s)$ and $D_f(s)$. As before, $s = i2\pi f$ is the complex frequency.

Reciprocity (namely $A_f D_f - B_f C_f = 1$) does not hold for forward transduction since this 2-port model is analogous to a transistor, as shown in the right panel of Fig. 24 (a transistor is not reciprocal) [32] [p. 254]. The parameters r and c in Fig. 24 represent the cilia stiffness and drag due to the fluid, while the parameters R_m and C_m represent the membrane resistance and capacitance. The current induced into the cell depends

[13] A dot over a variable indicates a derivative with respect to time, namely $\dot{x} = dx/dt$.

on channels in the cilia membrane. Following Fig. 24, the Thévenin equivalent current[14] $\dot{Q}_0(\xi_c)$, which depends on the displacement of the cilia ξ_c, is given by

$$\dot{Q}_0(\xi) = [g(\xi_c) + R_m + sC_m]V_0, \tag{22}$$

where V_0 is the equivalent battery voltage supplied to the cell by the stria vascularis and membrane batteries, $\dot{Q}_0$ is the Thévenin current, $g(\xi_c)$ is the conductance of the cilia, which is a function of the cilia displacement, and $1/R_m + sC_m$ is the membrane admittance.

Reverse transduction More important, from the modeling point of view, is the case of reverse transduction, for which the input is the membrane voltage V_m and current $\dot{Q}_m$, which represents the *output* of the forward transduction.

One output variable is the movement of the cell, which may be characterized in several ways. One possibility, with certain advantages, is to define the output flow variable to be the cell's fluid volume flow $\dot{\mathcal{V}}$. The conjugate variable to a fluid volume flow is the turgor pressure $\mathcal{P}$ (effort). The resulting $ABCD$ transmission matrix equation that specifies outer hair cell reverse transduction equation is[15]

$$\begin{bmatrix} \mathcal{P} \\ \dot{\mathcal{V}} \end{bmatrix} = \begin{pmatrix} A_r & B_r \\ C_r & D_r \end{pmatrix} \begin{bmatrix} V_m \\ \dot{Q}_m \end{bmatrix}. \tag{23}$$

It is frequently speculated (but not actually proven) that reciprocity holds for this system, namely that $A_r D_r - B_r C_r = 1$. Reciprocity is a sufficient condition that the system may be run in reverse, with pressure and flow as the input, and voltage and current as the output, analogous to a piezoelectric crystal.

Given the cell turgor pressure and volume velocity (Eq. 23), we need to find the cells axial force F_z (effort) and strain ϵ_l (relative length change). Relationships have been formulated between the longitudinal ϵ_l and circumferential ϵ_c strains, the axial applied force F_z, and the turgor pressure $\mathcal{P}$ [146]. Before presenting this equation of motion, a few definitions are necessary.

Definitions. The longitudinal strain ϵ_l is defined as the change in length L, per unit length. If the cell's length changes by δL, then $\epsilon_l \equiv \delta L/L$. This variable is useful because, for a given force, the strain is a local (i.e., a density) description of the movement. Likewise $\epsilon_c \equiv \delta C/C$ is the relative change of the circumference $C = 2\pi R$, where R is the cell radius. From the basic definition of a strain, $\epsilon_r = \epsilon_c$.

The longitudinal T_l and circumferential T_c stress are defined as the force normalized by the length (or area) over which the force is applied. The axial membrane stress T_z is therefore the area of the cell's end cap πR^2 times the pressure $\mathcal{P}$, divided by the circumference $2\pi R$, plus the applied axial stree F_z/C, namely $T_z = R\mathcal{P}/2 + F_z/C$. The circumferential stress T_c is given by the tension in the membrane generated by the turgor pressure $\mathcal{P}$ pushing on the membrane wall ($\mathcal{P}2LR$), normalized by the length ($2L$), giving $T_c = R\mathcal{P}$ [144, 147].

In general four coefficients of elasticity relate the two strains ϵ_l and ϵ_c and two stress T_z and T_c. Elastic system are reciprocal, reducing the number of constants from four to

[14] This may also be called the "Norton equivalent current."

[15] Note that the signal variables must be the *small signal component* of each variable. In other words, the mean value is subtracted from each of these state variables.

three. These three constants (e_l, e and e_c) must be determined experimentally. As shown by Iwasa, the resulting Hooke's law (stress-strain) equation of motion for the cell is [146]

$$\begin{pmatrix} e_l & e \\ e & e_c \end{pmatrix} \begin{bmatrix} \epsilon_l \\ \epsilon_c \end{bmatrix} = \begin{bmatrix} R\mathcal{P}/2 + F_z/C \\ R\mathcal{P} \end{bmatrix}. \tag{24}$$

"Stress" and "strain" terms have been grouped, as in an *impedance matrix* formulation. Strain is used rather than strain rate (i.e., $\dot{\epsilon}$), because the equation is static. If viscosity had been included this would necessarily change. The *output* axial force F_z is coupled with the *input* turgor pressure $\mathcal{P}$ on the right hand side of the matrix equation, while the two strains ϵ_l and ϵ_c are paired on the left hand side of the equation.

After some algebra, the *stress-strain* Iwasa's Eq. 24 may be reduced to transmission matrix form. In doing this ϵ_c may be rewritten in terms of the volume strain $\epsilon_v = \delta\mathcal{V}/\mathcal{V}$ to make it similar to the left hand side of Eq. 23, by using $\epsilon_c = (\epsilon_v - \epsilon_l)/2$. It is also necessary to convert to strain rates ($\dot{\epsilon}_l$ and $\dot{\epsilon}_v$) since we wish to match the units of Eq. 23. Conversion to strain rate introduces the complex frequency $s = i2\pi f$ in the lower left element of the matrix which operates on the turgor pressure, in this equation. We also use the identities $\dot{\epsilon}_v = \dot{\mathcal{V}}/\mathcal{V}$ and $\dot{\epsilon}_l = \dot{L}/L$.

$$\begin{bmatrix} F_z \\ \dot{L} \end{bmatrix} = \begin{pmatrix} \frac{e_l - e + e_c/4}{2e - e_c} 2RC & \frac{e_l e_c - e^2}{2e - e_c} C/\mathcal{V}s \\ \frac{s}{2e - e_c} 2RL & \frac{e_c}{2e - e_c} L/\mathcal{V} \end{pmatrix} \begin{bmatrix} \mathcal{P} \\ \dot{\mathcal{V}} \end{bmatrix}. \tag{25}$$

This equation relates the turgor pressure and the cell fluid volume flow to the axial force and velocity. Due to the splitting of T_z into its two components ($R\mathcal{P}/2$ and F_z/C), this system is not reciprocal, even though Eq. 24 is. The cascade of the two transmission matrices Eqs. 23 and 25 provides a description of reverse transduction from the electrical input to the longitudinal output.

3.2.2 Physics of the OHC

Given the basic equations of reverse transduction Eqs. 23 and 25, the coefficients must be determined from physical measurements and models of the OHC membranes. It must be determined experimentally if $B_r = C_r$ [31].

Conservation of cell volume. Based on data from Ashmore, Iwasa and Chadwick [144] pointed out that the volume of the cell must be constant (i.e., $\dot{\mathcal{V}} = 0$) over acoustic time scales. This condition follows from fluid mass conservation (due to fluid viscosity, the membrane cannot pass fluid over these short time scales). Therefore a change in membrane voltage cannot change the volume of fluid in the cell. As shown by Eq. 25, if the pressure were also constant, the cell length could not change.

The cylindrical shape of the OHC is significant, in the following sense. If the cell were a sphere, and its volume were constant, then it could not move. This effect has been used to advantage by Adachi and Iwasa [148]. A sphere has the minimum volume to area ratio, giving it special properties. Its volume and area both depend on the radius, making it a highly symmetric structure. The cylindrical OHC depends on two dimensions, R and L. Given a constant volume, unlike the sphere, the area and length *can* change. If OHCs were spheres, the inner ear could not work!

Relation between length and area variation. The relation between the length and radius strain may be determined by assuming that the cell volume $\mathcal{V}$ is constant over one cycle of the stimulus (i.e., $\dot{\mathcal{V}}$ = 0), and that it has a fixed cylinder shape. Setting to zero the variation (a small change) in the log volume

$$\delta \log(\mathcal{V}) = \delta \log(R^2 L) = 0 \tag{26}$$

leads to [149]

$$\epsilon_r = -\sigma \epsilon_l, \tag{27}$$

with $\sigma = 1/2$.

The negative of the ratio of the radius strain to length strain is called the *Poisson ratio* σ. Feynman points out that the Poisson ratio is between 0 and 1/2 [149]. The value of $\sigma = 1/2$ occurs with incompressible homogeneous volumes, as in Eq. 27.

Experimental pipette results. Experimental details on the relations between OHC length L, radius R, volume $\mathcal{V}$, and turgor pressure $\mathcal{P}$, have been quantified by Iwasa and Chadwick (1992) [144]. They measured the fractional cell length and radius change (ϵ_l, ϵ_r) as a function of the turgor pressure by placing a pipette in a cell and varying the volume and pressure. They experimentally found that

$$\epsilon_r = -\sigma \epsilon_l \tag{28}$$

with 1.85 $< \sigma <$ 2.3,[16] and

$$\epsilon_l = -G\mathcal{P}, \tag{29}$$

with $G \approx 0.07$ (kPa)$^{-1}$. The resulting volume strain for this case is

$$\frac{\delta \mathcal{V}}{\mathcal{V}} \equiv 2\epsilon_r + \epsilon_l = (2\sigma - 1) G\mathcal{P} \approx 0.28\mathcal{P}. \tag{30}$$

These two measurements allowed Iwasa and Chadwick to estimate the cell membrane's elastic properties. Assuming the membrane is isotropic, they found that *bulk modulus* $K = 0.07$ N/m, and *shear modulus* $\mu = 0.007$ N/m.[17] Assuming whole cell isotropy, Iwasa found that $e_l = e_c = K + \mu$, and $e = K - \mu$ [145], giving direct estimates of these two important parameters. Steele *et* al. showed that the whole cell is not isotropic however, and found the ratio of $e_c/e_l = 3.5$ [150]. These estimates remain controversial.

For both the iso-volume and pipette cases the length of the cell decreases as the radius and pressure increase. In the iso-volume case (Eq. 27), the Poisson ratio is $\sigma = 1/2$, as required. In the pipette case Eq. 28, $\sigma \approx 2$. According to Feynman the maximum physical value of the Poisson ratio σ is 1/2, yet in the pipette experiment it is approximately 2. In the next section a simple explanation of this "impossible" experimental result is provided.

Model of the pipette results. Consider two cylinders having a common axis but slightly different radii, $R_2 > R_1$. The volume of the fluid between two such cylinders $\mathcal{V}_{12}$ is given by

$$\mathcal{V}_{12} = \pi(R_2^2 - R_1^2)L \tag{31}$$

$$= 2\pi \left[\frac{R_1 + R_2}{2}\right](R_2 - R_1)L. \tag{32}$$

[16] They report 1/σ = 0.43 in the Fig. 1 caption, while 1/σ = 0.58 may be inferred from their Fig. 2 caption using their Eq. 3.

[17] For a lucid definition of these coefficients, see [149].

Define thickness $T \equiv R_2 - R_1$, mean radius $R \equiv (R_1 + R_2)/2$, and length L. Using this notation, the volume is given by $\mathcal{V}_{12} = 2\pi RTL$. As before, assume that the volume $\mathcal{V}_{12}$ is constant, and set to zero the variation of the log volume

$$\delta(\log \mathcal{V}_{12}) = \left[\epsilon_t + \frac{1}{2}\epsilon_r\right] + \left[\frac{1}{2}\epsilon_r + \epsilon_l\right] = 0. \tag{33}$$

The experimental observation of Eq. 28 says that the second quantity in square brackets is zero. Therefore the first quantity in square brackets must also be zero, and $\epsilon_t = \epsilon_l$, (resulting in an experimental prediction). It is helpful to think of a circumferential "ring" slice of hair cell as a bar, with its ends abutted, and Eq. 28 follows naturally. When the cell is sealed the roles of C and L reverse, so effectively σ goes from 2 to 1/2 due to the geometrical modification.

The longitudinal strain versus voltage. The length of the cell L is known to be a function of the turgor pressure $\mathcal{P}$ and the membrane voltage V_m, namely $L(\mathcal{P}, V_m)$ [144, 148, 79, 80]. The linearized small–signal change in length δL must be of the form

$$\delta L(\mathcal{P}, V_m) = \mathcal{C}(V_m)\mathcal{P} + m_0 V_m, \tag{34}$$

where from Eq. 25 (assuming $\dot{\mathcal{V}} = 0$),

$$\mathcal{C}(V_m) = \frac{2R}{e_c + 2e}$$

chacterizes the soma trans-compliance per unit area in the axial direction. Constant m_0 is defined as the longitudinal strain *motor* sensitivity, which characterizes the axial component of the "area motor" strength [151]. The cell trans–compliance per unit area $\mathcal{C}(V_m)$ is a function of membrane voltage V_m, as reported by He and Dallos [79, 80]. If we make the small–signal approximation

$$\mathcal{C}(V_m) \approx c_0 + c_1 V_m,$$

then $c_1 \neq 0$. In other words, one or both of e_l and e_c must depend on the membrane voltage.

The justification for the form of Eq. 34 is as follows: If the voltage and pressure change are zero ($\dot{V}_m = 0$, $\dot{\mathcal{P}} = 0$), then $\dot{L} = 0$. If the turgor pressure alone is varied, the length varies in proportion to the passive longitudinal trans-compliance per unit area c_0. In the general case, a change in the soma voltage V_m will have a complex effect on the cell. Both the area motor [151] and the voltage dependent cell wall induced longitudinal compliance $\mathcal{C}(V_m)$ [79, 80] will contribute to the area change. Any relative area change ϵ_a, due to the area motor, must induce a volume conserving corresponding length change $\epsilon_l = 2\epsilon_a$. These two sources of length change are then added on the right hand side of Eq. 34.

4 Micromechanics

Unlike the case of macromechanical models, the physics of every micromechanical model differs significantly. This is in part due to the lack of direct experimental evidence of physical parameters of the cochlea.

To organize our discussion of cochlear micromechanics, we represent each radial cross-section through the cochlear partition as a linear 2-port network. A general formalization in transmission matrix form of the relation between the basilar membrane *input* pressure $P(x,s)$ and velocity $V(x,s)$ and the OHC *output* cilia bundle shear force $f(x,s)$ and shear velocity $v(x,s)$

$$\left[\begin{array}{c} P \\ V \end{array} \right] = \left(\begin{array}{cc} A & B \\ C & D \end{array} \right) \left[\begin{array}{c} f \\ \dot{\xi} \end{array} \right], \tag{35}$$

where A, B, C, and D are complex functions of place x and radian frequency s. If we knew the functions A, B, C, D as a function of frequency and place, many of the current questions about modeling cochlear micromechanics would be answered.

The complex ratio of the force $f(x,s)$ (effort) on the cilia bundle to the velocity $\dot{\xi}(x,s)$ (flow) defines the load impedance Z_c. The cilia bundle impedance is assumed to be composed of a mass M_c, stiffness K_c, and viscous fluid drag in the 6-10 μm space between the tectorial membrane and the reticular lamina, represented by R_c, namely

$$\frac{f}{\dot{\xi}} \equiv Z_c(x,s) = sM_c + R_c + K_c/s. \tag{36}$$

Partition transduction. As previously discussed, an important question in cochlear mechanics is the extent to which the tuning of the basilar membrane (at a given place) determines the tuning of the cilia bundles of the IHCs and OHCs. We will define H_c, the *transduction filter,* to be the complex ratio of the OHC cilia bundle velocity to basilar membrane velocity, as a function of frequency. In terms of the transmission matrix (and load impedance),

$$\frac{\dot{\xi}}{V} \equiv H_c(x,s) = 1/(CZ_c + D). \tag{37}$$

The amount of additional tuning (filtering) provided by H_c is a longstanding *open* experimental question. Micromechanical models explore at the heart of this uncertainty.

Partition impedance. In terms of the general transmission matrix parameters, the partition impedance used in the macromechanical models (Eq. 9) is given by

$$\frac{P}{V} \equiv Z_p(x,s) = (AZ_c + B)/(CZ_c + D) \tag{38}$$

$$= H_c(AZ_c + B). \tag{39}$$

Some of the assumptions of macromechanical models that can be studied are (a) the effect of geometrical relationships on the cochlear partition impedance and cilia motions (e.g. stiffness of the OHC), (b) the effect of parameter relationships on the cochlear partition impedance and cilia motions (e.g. importance of K_t/K_c), (c) the effect of nonlinear elements (e.g. length and stiffness of the OHC soma as a function of its voltage), and (d) the effect of adding mechanical degrees of freedom.

Figure 25 shows a simplified version of the radial cross-section geometry of Fig. 2. If we assume that the tectorial membrane is elastic between the place where it contacts the hair cells and its attachment to the bony spiral limbus (K_t), then a significant enhancement of tuning between the basilar membrane and the IHC necessarily follows, as given in Eq. 37. This is the basis of the *resonant tectorial membrane* (RTM) model [22] discussed next, and

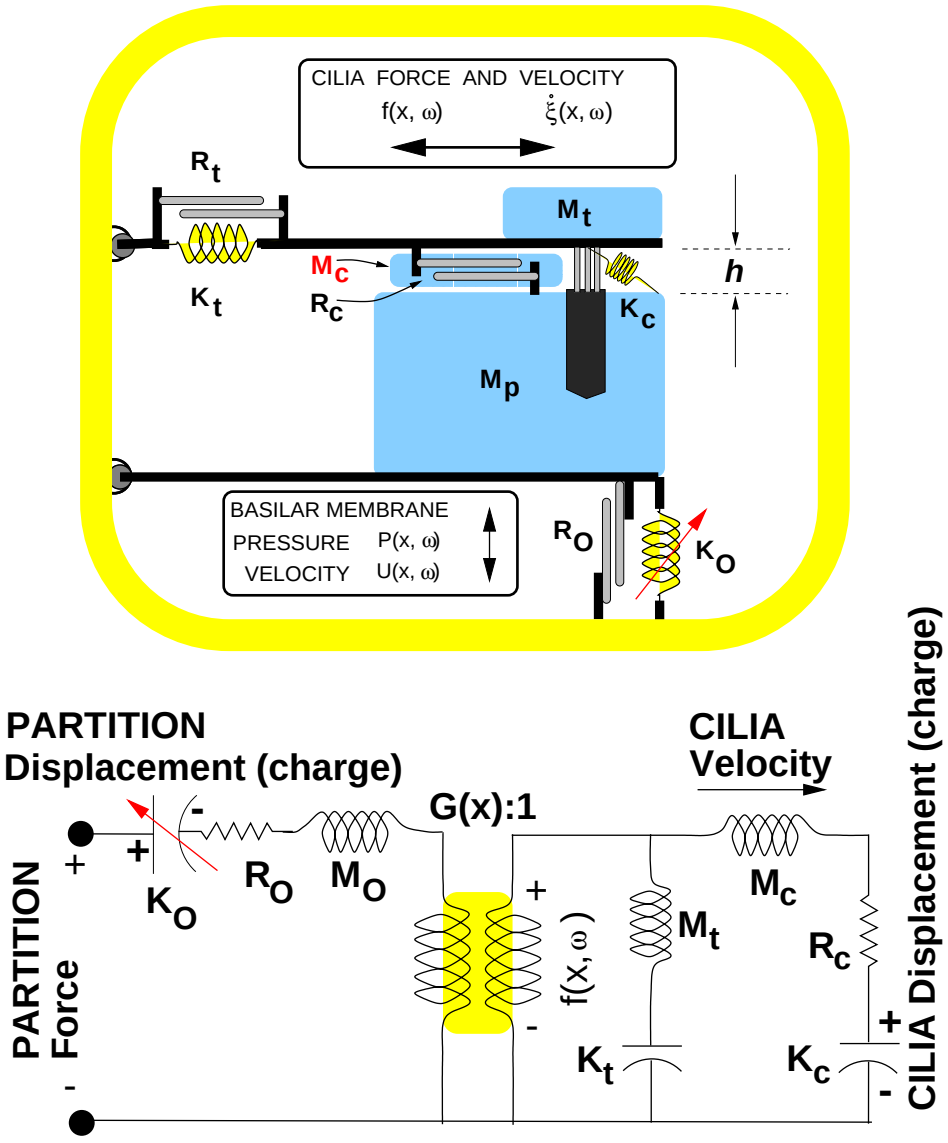

Figure 25: *Shown here is the basic RTM model of the cochlear partition radial cross-section. In this drawing, the mass of entire organ of Corti is lumped into M_b and the tectorial membrane is represented by M_t (see Fig. 2). The two masses are coupled to each other by mass M_c, compliance K_c, and damping R_c. The tectorial membrane is attached to bone by K_t and R_t and the basilar membrane by K_b and R_b. The arrow through the spring K_{OHC} represents the voltage dependent stiffness of the outer hair cell soma. The cilia mass M_c has a huge effect on slope S_2 (see top panel of Fig. 27). The lower half of the figure shows the electrical equivalent circuit which is a convenient starting point for writing equations. This representation of the cochlear partition is a common starting point for modeling cochlear micromechanics.*

is an example of passive enhancement of cochlear tuning. If we assume that the motility of OHCs can be modeled as a controlled source of mechanical energy between the basilar membrane and the reticular lamina, then we have the ingredients for active enhancement of cochlear tuning such as in the *cochlear amplifier* (CA) model.

Active and passive models currently represent two alternative and competitive explanations of cochlear mechanics. *Active* models contain sources of mechanical energy and passive models do not. In some sense passive models are "active," because the cochlea has a battery, and therefore the cochlea is active. However this is not how the term "active" is being used here, in keeping with popular usage. The generic term *active model* does *not* capture either the intent nor the physics of the CA model, and is inappropriate nomenclature. Any system containing a source of power (i.e., a battery) is, by definition, active. The cochlea *is* active, since it has a battery. However the question of whether the OHC's provide power amplification to the basilar membrane traveling wave (i.e., is there a CA) is very much an open question.

4.1 Passive BM models

The most successful *passive* model of cochlear tuning is the resonant tectorial membrane (RTM) model [22, 13]. The RTM model starts from the assumption that the slope S_2 of BM tuning is insufficient to account for the slope S_2 of neural tuning, as seen in Tab. 1. This sharpening is accounted for by a reflection in the tectorial membrane, introducing an antiresonance (*spectral zero*) at frequency F_z, which about half an octave below the resonant frequency F_{cf} of the basilar membrane, into H_c Eq. 37.

From Fig. 25, and as described by Allen and Neely (1992), the A, B, C, D elements of Eq. 35 are given by [22, 13]:

$$A = G + Z_b/GZ_t \quad (40)$$
$$B = Z_b/G \quad (41)$$
$$C = 1/GZ_t \quad (42)$$
$$D = 1/G, \quad (43)$$

where G is the ratio of the OHC cilia bundle displacement and the BM displacement when $Z_c = 0$, $Z_b = sM_b + K_{ohc}/s$ is the BM impedance, $Z_c = sM_c + R_c + K_c/s$, and $Z_t = sM_t + K_t/s$ is the TM impedance. These element definitions are illustrated in Fig. 25. For this discussion we shall assume that $G = 1$.

In this model the OHC transduction filter (Eq. 37)

$$H_c(x,s) = G\frac{Z_t}{Z_c + Z_t} \quad (44)$$

is a high-pass filter with a low-frequency attenuation given by $GK_t/(K_t + K_c)$. A key issue here is the magnitude of the impedance ratio $|Z_t/Z_c|$, which in practice depends on the stiffness ratio K_t/K_c. If this ratio is greater than 1, then the basilar membrane and OHC tuning will be similar (they will differ only by G which does not vary with frequency). If the ratio is less than 1, then the tuning may differ.

Of equal importance is the partition input impedance $Z_p(x,s)$ given by Eq. 39

$$Z_p(x,s) = Z_b + G^2\frac{Z_cZ_t}{Z_c + Z_t}, \quad (45)$$

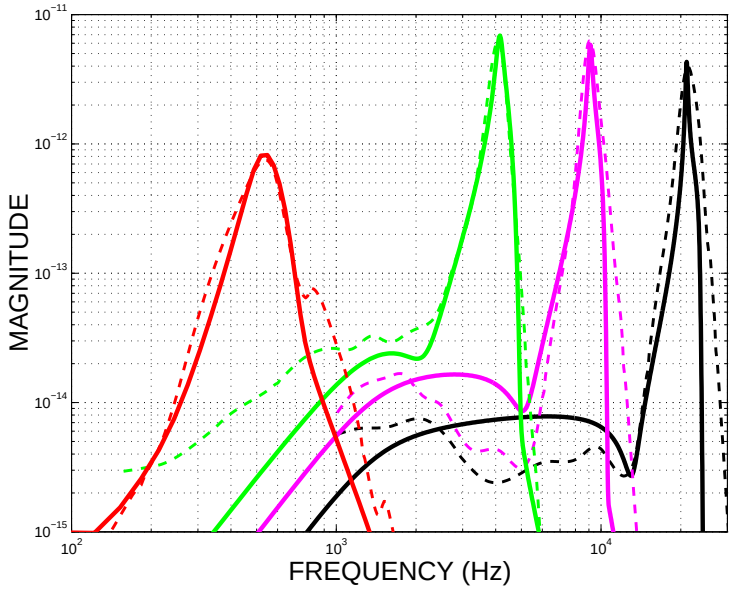

Figure 26: *Comparison between neural data and the computed model excitation patterns from Allen's passive RTM model. These results used a linear version of the model.*

which determines the tuning of the basilar membrane.

The response ratio of IHC cilia bundle displacement to basilar membrane displacement is [67]

$$H_{ihc}(x,s) = \frac{s}{s + i2\pi f_0} H_c(x,s), \tag{46}$$

where f_0 is the frequency above which the cilia bundle of the IHC follows fluid displacement rather that fluid velocity, as determined by the IHC drag and cilia bundle stiffness. Dallos has determined this frequency to be $f_0 \approx$0.8 kHz [2]. The parameters of the RTM model may be chosen such that model results for mechanical input to the IHC fit the experimental neural threshold tuning curves closely, as shown in Fig. 26.

4.1.1 The nonlinear RTM model.

The RTM model is made nonlinear by control of the BM stiffness via OHC's stiffness (or length changes) [78, 152, 153], as shown in Figs. 2 and 25. The basal end of each OHC is attached to the BM via an interlaced chain of Dieter cells. Attached to the apical end of the OHCs are the cilia, the longest row of which are connected to the TM.

It is postulated that the decrease in OHC stiffness, accompanying cilia stimulation, results in a decrease of the net partition stiffness $K_p(x)$ (increasing compliance). As shown in Fig. 27, this decrease in the local BM stiffness results in the partition excitation pattern shifting basally towards the stapes. Another way to view this, shown in the bottom of panel of Fig. 27, is that at any point x along the BM, the resonant frequency F_{cf} decreases with increasing intensity. This migration of the excitation pattern, combined with the assumption that the TM has a highpass characteristic, means that the cilia excitation gain at CF is nonlinearly compressed as the intensity increases. This compression effect is shown in

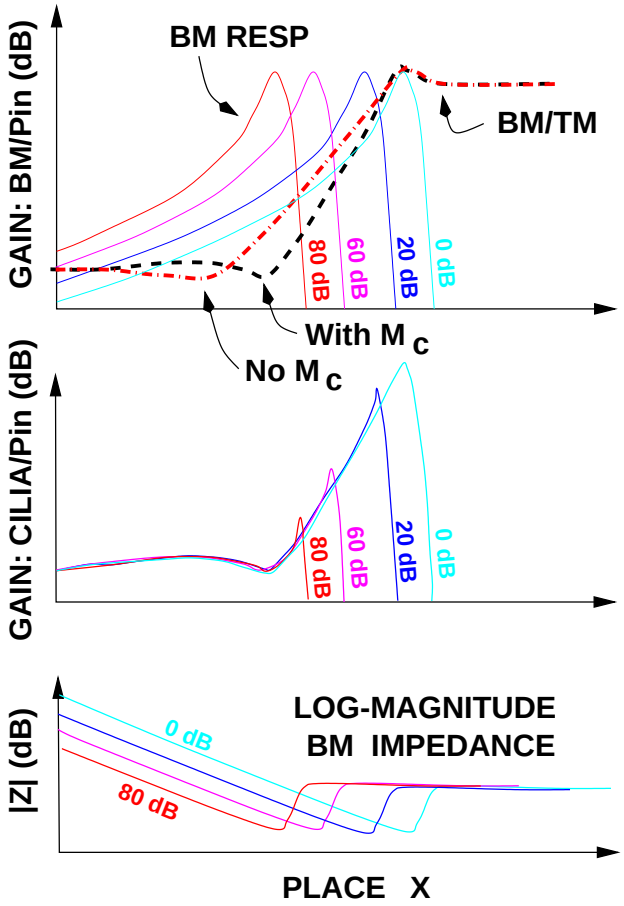

Figure 27: *This "cartoon" figure depicts the method by which the model's voltage controlled basilar membrane stiffness changes the cochlear gain as a function of level. In each panel the stimulus is a wideband noise, at four intensities between 0 and 80 dB SL. Each response is normalized, and is shown in dB, as a function of place. In the top panel we see the BM normalized by the ear canal pressure transfer function, with the input tone's intensity as the parameter (solid lines). The BM to TM transfer function is shown as a dashed line. In the center panel we show the composite response, the cilia response normalized by the ear canal pressure. In the bottom panel we display the BM impedance magnitude for various intensities.*

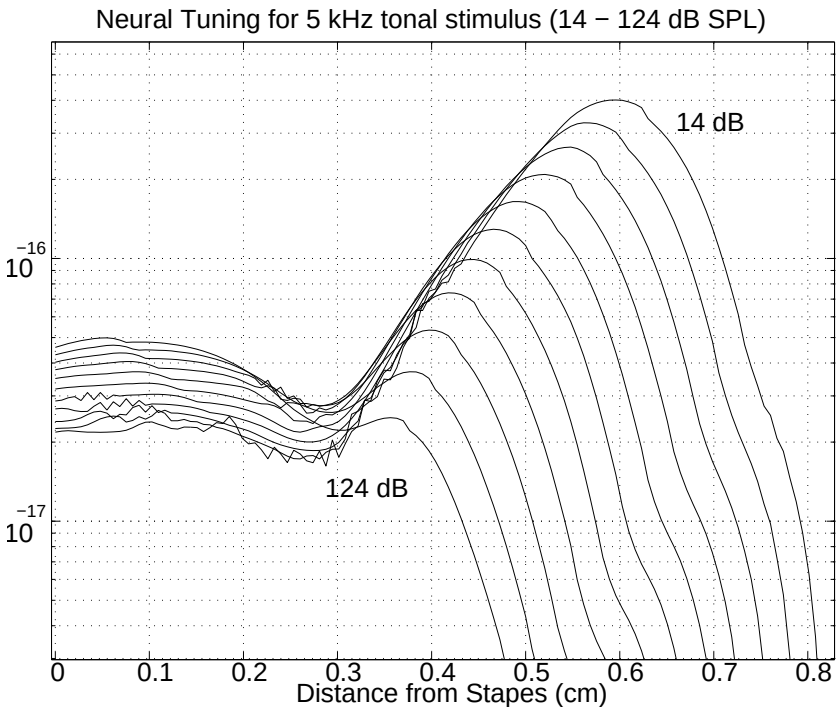

Figure 28: *Compression in the NL-RTM model.*

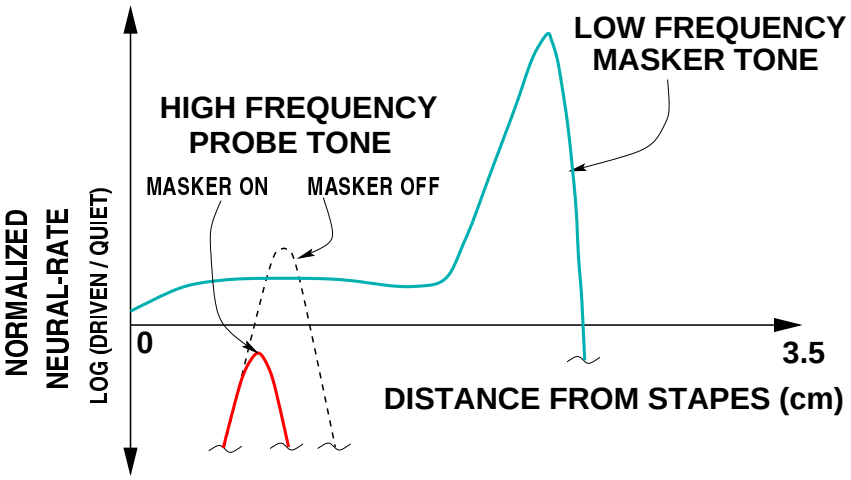

Figure 29: *Cartoon showing the effect of a low frequency masker on a high frequency tone as a function of position along the basilar membrane. The horizontal line at the origin along the ordinate represents the hearing threshold in quiet.*

a cartoon format in Fig. 29, while Fig. 28 shows the actual calculated model results. Note how the bandwidth (ERB) remains approximately constant as a function of input intensity.

Discussion. Two important advantages of the NL-RTM model include its physically based assumptions (described above), and its simplicity. Given these physical assumptions, we show next that the NL-RTM model can explain: a) the basalward half-octave traveling wave migration as a function of increasing intensity [99], b) the upward spread of masking (USM) [16, 81], two-tone suppression (2TS) (see Sec. 2.2.5), d) distortion product generation [56, 82, 154, 83, 155, 156], e) normal and recruiting loudness growth, and f) hypersensitive tails [43].

From the steep 2.4 dB/dB slope of the USM and 2TS (Fig. 18) it seems necessary that the low frequency suppressor is turning down the high frequency probe even though the growth of the masker at the high frequency's place is linear with masker level, as shown in Fig. 29.

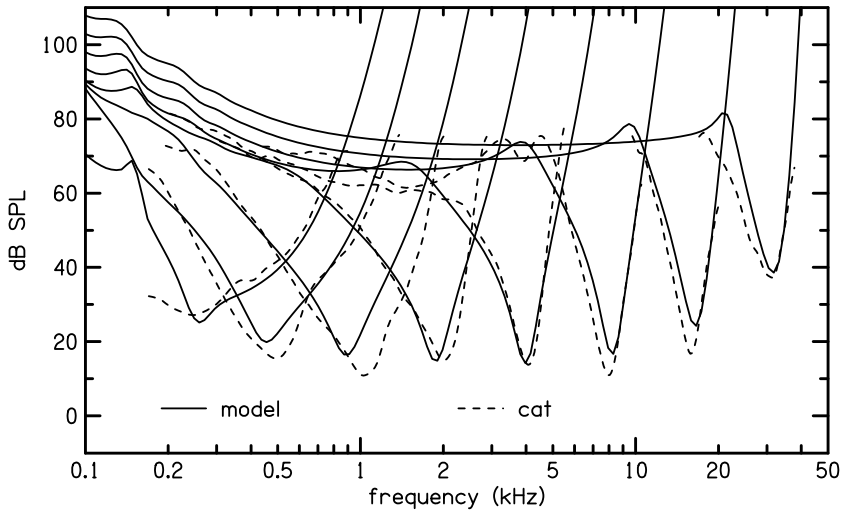

Figure 30: *Comparison between neural data computed tuning curves from Neely's active model [157]. This CA model assumes an IHC cilia bundle displacement of 300 picometers at the neural rate threshold. The tuning curves shown by the dashed lines are the average of single nerve fiber responses from six cats obtained by M. C. Liberman and B. Delgutte.*

4.2 Active BM models

One obvious question about active cochlear models is "Are they really necessary?" At least three attempts to answer this question based on detailed comparisons of basilar membrane responses have concluded that the measured responses *cannot* be account for by a passive cochlear model [158, 134, 159, 160, 161]. On the other hand, one study concluded that cochlear amplifier (CA) models are inconsistent with experimental distortion product data measured in the ear canal [135].

4.2.1 The CA hypothesis

The most popular micromechanical theory is called the *cochlear amplifier* (CA) hypothesis. The concept of the *cochlear amplifier*, originated by Gold, Kemp, Kim and Neely, and named by H. Davis, refers to a hypothetical mechanism within the cochlear partition which increases the *sensitivity* of basilar membrane vibrations to low level sounds and, at the same time, increases the *frequency selectivity* of these vibrations [162]. The CA adds mechanical energy to the cochlear partition at acoustic frequencies by drawing upon the electrical and mechanical energy available from the outer hair cells. In response to a tone, the CA adds mechanical energy to the cochlear traveling wave in the region defined by S_2 as it approaches the place of maximum response. This energy is reabsorbed at other places along the cochlear partition. The resulting improvement in sensitivity of the ear due to the CA is thought to be 40 dB, or more under certain conditions; however, the details of how this amplification might be accomplished are still unknown. A general discussion of this model is presented in Dan Geisler's 1998 book [110] and in Allen and Fahey (1992).

It is presumed that this OHC action amplifies the BM signal energy on a cycle-by-cycle basis, increasing the sensitivity [94, 133]. In some of the models it is assumed that this cycle-by-cycle pressure (force) due to the OHCs causes the sharp BM tuning tip. In most of these models, the CA is equivalent to introducing a frequency dependent negative damping (resistance) into the BM impedance. Nonlinear compression is introduced by assuming that the resistance is signal level dependent. This NL resistance model was first described by Hall [64] for the case of $R > 0$. Thus the CA model is an extension of Hall's model to the case of $R < 0$. In several models nonlinear negative damping is obtained with a nonlinear stiffness and a small delay. The addition of a small delay introduces a negative real part into the impedance.[18] CA models models do not depend on a loosely coupled or resonant TM, but some do use micromechanical mechanisms to assist in the tuning.

Cochlear amplifier models generally have a region where the real part of the impedance of the cochlear partition becomes negative. It makes sense that this region correspond to the high slope portion of the tuning curve defined by S_2 defined in frequency as $F_z < f < F_{cf}$, because this is where the traveling wave slope changes [135]. As the traveling wave generated by a sinusoidal stimulus encounters a region of negative damping, the power of the traveling wave will increase abruptly. In the negative damping regions, the pressure across the basilar membrane also increases, relative to the passive case. Zweig (1991) [134] has developed a ingenious negative-damping model based on the experimental data of Rhode which is perhaps the most detailed of these negative-damping models.

Hybrid CA models can include both negative-damping elements in the cochlear partition and a resonant tectorial membrane. For example, in Neely and Kim's active model [133], B of Eq. 41 was replaced by $B' = B - \gamma Z_4$. This model is active for $\gamma > 0$. The use of negative damping elements is to (a) increase the sharpness of tuning of the BM responses, both in relative frequency response and amplitude sensitivity at the best frequency, and (b) provide larger cilia bundle displacements to the IHC as shown in Fig. 30. These CA models can achieve sharp tuning while maintaining stability, in the sense that transients responses decay with time.

Another view of active elements is that they provide the gain for a mechanical feedback loop [163]. For example, Mountain and Hubbard assume $G = 1$ and $Z_t \gg Z_c$ and that the cilia bundle stiffness K_c (Eq. 36) depends on the OHC voltage. Based on the 90 degree

[18] In mathematical physics, nonlinear damping resonators are called *van der Pol equations*, while nonlinear stiffness resonators are call *Duffing equations* [30].

phase shift resulting from the OHC membrane capacitance, they developed a theory in which R_c (Eq. 36), the effective cilia bundle resistance, becomes negative for frequencies greater than the membrane cutoff frequency f_m, but remains positive for $f < f_m$.

Geisler also proposed a feedback model [164] where the cell body of the OHC is modeled as a spring having an impedance $Z_r = K_r/s$, in series with an active force generator. However, this model leads to a physically unrealizable system of equations.

4.3 Discussion

Both active and passive BM models are reasonably successful at simulating the neural threshold response tuning curves. Thus we need to look elsewhere to contrast the difference between these two approaches, such as 2TS/USM. While the passive RTM model is easily made nonlinear with the introduction of $K_{ohc}(V_m)$, differences between *nonlinear* RTM and CA models have not yet been investigated. The CA and RTM models differ in their interpretation of damaged cochlear responses. In CA models, the loss of sensitivity of the cochlea with damage is interpreted as a loss of CA gain while in passive models, the loss of sensitivity has been interpreted as a 2:1 change in the BM stiffness [130].

The discovery of OHC motility demonstrates the existence of a potential source of mechanical energy within the cochlear partition which is suitably positioned to influence vibrations of the basilar membrane. It is still an open question whether this source of energy is sufficient to power a CA at high frequencies.

One possible advantage of the CA is that of improving the signal-to-noise ratio in front of the IHC detector. A weakness of the CA models has been their lack of specificity about the physical realization of the active elements. Until we have a detailed physical representation for the CA, RTM models have the advantage of being simpler and more explicit.

The discovery by He and Dallos that the OHC soma stiffness is voltage dependent is an exciting development for the nonlinear passive RTM model, as it greatly simplifies the implementation of the physical model. The RTM model has been in disfavor because many feel it is does not account for basilar membrane tuning. This criticism is largely due to the experimental results of physiologists who have measured the BM-ear canal transfer function, and found the tuning of BM velocity to be similar to neural threshold response data. Much of the experimental BM data, however, are not convincing on this point, with the BM slope S_2 generally being much smaller than that of neural responses. The question of whether an active model is required to simulate measured BM responses is still being debated.

Better estimates of the amplitude of cilia bundle displacement at a given sound pressure level directly address the sensitivity questions. If the estimate of Russell Sec. 3.1.2 of 30 mV/degree is correct, then the cochlear sensitivity question may be resolved by having very sensitive detectors. Also, better estimates are needed of the ratio of the BM frequency response to the IHC frequency response, both at high and low frequencies. Rhode's approach of using the slopes of Fig. 9 rather than Q_{10} might be a useful tool in this regard.

5 Summary

This paper has exhaustively reviewed what we know about the cochlea, which is a complex topic. Hopefully this has provided a framework to help the reader glue the various pieces of the puzzle together, thereby simplifying the subject.

The *Introduction* section reviews the nature of modeling and briefly describes the anatomy of the inner ear, and the function of inner and outer hair cells. In Sec. 1 we reviewed the history of cochlear modeling. The Wegel and Lane paper was a key paper that introduced the first detailed view of masking, and in the same paper introduced the first modern cochlear model Fig. 4. In Sec. 1.2.1 we presented the basic tools of cochlear modeling, *impedance*, the *Thévenin circuit*, and the *Transmission matrix* method (2-port analysis). In Sec. 1.3.1 we describe how these models work in intuitive terms, where the basilar membrane is treated as having an acoustic hole in it, that depends on frequency. The location of the hole, as a function of frequency, is called the cochlear map. This hole keeps fluid from flowing beyond a certain point, producing the cochlear traveling wave.

In Sec. 2 we extensively review and summarize the nonlinear measures of cochlear response. Since these data are not fully understood, and have not be adequately modeled, this is the most difficult section. However it is worth the effort to understand these extensive data and to appreciate the various relations between them, such as the close parallel between two–tone suppression and the upward spread of masking, and between loudness recruitment and outer hair cell damage.

In Sec. 3 we review several models of the hair cell, including forward and reverse transduction. Some of this material is recently published, and the view of these models could easily change over the next few years, as we better understand reverse transduction.

Finally in Sec. 4 we review the basics of micromechanics. We have presented the two basic types of models, *Passive* and *Active* models, with a critical review of each.

I would like to thank Paul Fahey for his reading of this paper, and for finding many errors. Sec. 3.2 could not have been written without the generous help of Kuni Iwasa. I did not always take his wise advice, and any errors are due to me alone. Section 4 is an update, based on [13], which was written in collaboration with Stephen Neely.

References

[1] J. O. Pickles. *An introduction to the physiology of hearing*. Academic Press Inc., London, England, 1982.

[2] P. Dallos. Cochlear neurobiology. In P. Dallos, A.N. Popper, and R.R. Fay, editors, *The cochlea*, pages 186–257, New York, 1996. Springer.

[3] S. Hecht. Vision II. the nature of the photoreceptor process. In C Murchison, editor, *Handbook of General Experimental Psychology*. Clark University Press, Worcester, MA, 1934.

[4] G.A. Gescheider. *Psychophysics: The Fundamentals, 3d edition*. Lawrence Erlbaum Associates, Mahwah, NJ; London, 1997.

[5] A.J. Hudspeth and D.P. Corey. Sensitivity, polarity, and conductance change in the response of vertebrate hair cells to controlled mechanical stimuli. *Proceedings National Academy Science*, 74(6):2407–2411, June 1977.

[6] J.C. Steinberg. Stereophonic sound-film system-pre- and post-equalization of compandor systems. *Journal of the Acoustical Society of America*, 13:107–114, October 1941. B-1327.

[7] R. Lorente de No. The diagnosis of diseases of the neural mechanism of hearing by the aid of sounds well above threshold. *Transactions of the American Otological Society*, 27:219–220, 1937.

[8] J.C. Steinberg and M.B. Gardner. Dependence of hearing impairment on sound intensity. *Journal of the Acoustical Society of America*, 9:11–23, July 1937.

[9] T. S. Littler. *The physics of the ear*. Pergamon Press, Oxford, England, 1965.

[10] W. A. Yost. *Fundamentals of Hearing, An Introduction*. Academic Press, San Diego, London, 1994.

[11] B. C. J. Moore. Frequency analysis and masking. In B.C.J. Moore, editor, *Hearing*, chapter 5, pages 161–205. Academic Press, London, New York, 1995.

[12] William M. Hartmann. *Signals, Sound, and Sensation*. AIP Press, American Institute of Physics, Woodbury, NY, 1997.

[13] J. B. Allen and S. T. Neely. Micromechanical models of the cochlea. *Physics Today*, 45(7):40–47, July 1992.

[14] H. L. F. Helmholtz. *Helmholtz's popular scientific lectures*. Dover, New York, 1962.

[15] H. L. F. Helmholtz. *On the sensations of tone*. Dover, New York, 1954. Original German Edition appeared in 1863.

[16] Harvey Fletcher. Physical measurements of audition and their bearing on the theory of hearing. *Journal of the Franklin Institute*, 196(3):289–326, September 1923.

[17] Harvey Fletcher. A space-time pattern theory of hearing. *Journal of the Acoustical Society of America*, 1(1):311–343, April 1930.

[18] O.F. Ranke. Theory operation of the cochlea: A contribution to the hydrodynamics of the cochlea. *Journal of the Acoustical Society of America*, 22:772–777, 1950.

[19] W. M. Siebert. Ranke revisited - a simple simple short-wave cochlear model. *Journal of the Acoustical Society of America*, 56:594–600, 1974.

[20] Thomas Gold. Hearing. *IEEE Transactions on Information Theory*, 1(1):125–127, February 1953.

[21] Harvey Fletcher. On the dynamics of the cochlea. *Journal of the Acoustical Society of America*, 23:637–645, November 1951.

[22] J. B. Allen. Cochlear micromechanics: A physical model of transduction. *Journal of the Acoustical Society of America*, 68(6):1660–1670, 1980.

[23] D.M. Freeman and T.F. Weiss. On the role of fluid inertia and viscosity in stereociliary tuft motion: analysis of isolated bodies of regular geometry. In J.B. Allen, J.L. Hall, A. Hubbard, S.T. Neely, and A. Tubis, editors, *Peripheral Auditory Mechanisms*, pages 147–154, Berlin, New York, 1986. Springer–Verlag.

[24] Sunil Puria. *A theory of cochlear input impedance and middle ear parameter estimation*. PhD thesis, City University of New York, January 1991.

[25] Sunil Puria and Jont B. Allen. A parametric study of cochlear input impedance. *Journal of the Acoustical Society of America*, 89(1):287–309, January 1991.

[26] J.J. Zwislocki. Theorie der schneckenmechanik. *Acta Otolaryngol. [supl.]*, page 72, 1948.

[27] J.J. Zwislocki. Theory of the acoustical action of the cochlea. *Journal of the Acoustical Society of America*, 22:779–784, 1950.

[28] Peterson L. C. and Bogert B. P. A dynamical theory of the cochlea. *Journal of the Acoustical Society of America*, 22:369–381, 1950.

[29] Harvey Fletcher. Acoustics. *Phys Today*, 4:12–18, December 1951.

[30] Louis A. Pipes. *Applied Mathematics for Engineers and Physicists*. McGraw Hill, NYC, NY, 1958.

[31] Lars Onsager. Reciprocal relations in irreversible processes. I. *Physical Review*, 37:405–426, February 1931.

[32] M.E. Van Valkenburg. *Network Analysis*. Prentice-Hall, Englewood Cliffs, N.J., 1964.

[33] D.C. Karnopp, D.L. Margolis, and R.C. Rosenberg. *System Dynamics: A unified approach*. John Wiley & Sons Inc., NY, 1990. Second revised edition.

[34] S.E. Voss, J.J. Rosowski, and W.T. Peak. Is the pressure difference between the oval and round windows the effective acoustic stimulus for the cochlea? *Journal of the Acoustical Society of America*, 100(3):1602–1616, September 1996.

[35] Harvey Fletcher and W.A. Munson. Relation between loudness and masking. *Journal of the Acoustical Society of America*, 9:1–10, 1937.

[36] Harvey Fletcher. Loudness, masking and their relation to the hearing process and the problem of noise measurement. *Journal of the Acoustical Society of America*, 9:275–293, April 1938.

[37] Harvey Fletcher. Auditory patterns. *Reviews of Modern Physics*, 12:47–65, May 1940.

[38] J.C. Steinberg. Positions of stimulation in the cochlea by pure tones. *Journal of the Acoustical Society of America*, 8:176–180, 1937. Cochlear map estimate; Monograph B-973.

[39] Donald D. Greenwood. Critical bandwidth and the frequency coordinates of the basilar membrane. *Journal of the Acoustical Society of America*, 33(10):1344–1356, October 1961.

[40] J. B. Allen. Harvey Fletcher's role in the creation of communication acoustics. *Journal of the Acoustical Society of America*, 99(4):1825–1839, April 1996.

[41] Harvey Fletcher. *Speech and Hearing in Communication*. Robert E. Krieger Publishing Company, Huntington, New York, 1953.

[42] M.C. Liberman. The cochlear frequency map for the cat: Labeling auditory-nerve fibers of known characteristic frequency. *Journal of the Acoustical Society of America*, 72(5):1441–1449, 1982.

[43] M.C. Liberman and L. Dodds. Single neuron labeling and chronic cochlear pathology III: Stereocilia damage and alterations of threshold tuning curves. *Hearing Research*, 16:55–74, 1984.

[44] G. Zweig, R. Lipes, and J. R. Pierce. The cochlear compromise. *Journal of the Acoustical Society of America*, 59(4):975–982, 1976.

[45] M. A. Viergever. *Mechanics of the inner ear, a mathematical approach*. PhD thesis, Delft University, Delft, The Netherlands, 1980.

[46] W.S. Rhode. Observations of the vibration of the basilar membrane in squirrel monkeys using the Mössbauer technique. *Journal of the Acoustical Society of America*, 49:1218–1231, 1971.

[47] N.Y.-S Kiang and E.C. Moxon. Tails of tuning curves of auditory-nerve fibers. *Journal of the Acoustical Society of America*, 55:620–630, 1974.

[48] M. Lesser and D. Berkley. Fluid mechanics of the cochlea. *J. Fluid Mech.*, 51(3):497–512, 1972.

[49] C.R. Steel. Behavior of the basilar membrane with pure-tone excitation. *Journal of the Acoustical Society of America*, 55(1):148–162, January 1974.

[50] J. B. Allen. Two-dimensional cochlear fluid model: New results. *Journal of the Acoustical Society of America*, 61(1):110–119, January 1977.

[51] M. M. Sondhi. Method for computing motion in a two-dimensional cochlear model. *Journal of the Acoustical Society of America*, 63(5):1468–1477, 1978.

[52] J. B. Allen and M. M. Sondhi. Cochlear macromechanics: Time-domain solutions. *Journal of the Acoustical Society of America*, 66(1):120–132, July 1979.

[53] R.J. Diependaal and M.A. Viergever. Point-impedance characterization of the basilar membrane in a three-dimensional cochlear model. *Hearing Research*, 11:33–40, 1983.

[54] E. deBoer. Short waves in three-dimensional cochlear models: Solutions for a 'block' model. *Hearing Research*, 4:53–77, 1981.

[55] P.M. Sellick and I.J. Russell. Intracellular studies of cochlear hair cells: Filling the gap between basilar membrane mechanics and neural excitation. In F. Naunton and C. Fernandez, editors, *Evoked electrical activity in the auditory nervous system*, pages 113–140. Academic Press, New York, 1978.

[56] D.T. Kemp. Stimulated acoustic emissions from within the human auditory system. *Journal of the Acoustical Society of America*, 64:1386–1391, 1978.

[57] W.E. Brownell, C.R. Bader, D. Bertran, and Y. de Rabaupierre. Evoked mechanical responses of isolated cochlear outer hair cells. *Science*, 227:194–196, 1985.

[58] W.S. Rhode. Some observations on cochlear mechanics. *Journal of the Acoustical Society of America*, 64:158–176, June 1978.

[59] I. Russell and P. Sellick. "intracellular studies of hair cells in the mammalian cochlea,". *J. Physiol.*, 284:261–290, 1978.

[60] J.L. Goldstein. Auditory nonlinearity. *Journal of the Acoustical Society of America*, 41(3):676–699, March 1967.

[61] J. L. Goldstein and N. Kiang. Neural correlates of the aural combination tone 2f1-f2. *Proc. of the IEEE*, 56:981–992, 1968.

[62] G.F. Smoorenburg. Combination tones and their origin. *Journal of the Acoustical Society of America*, 52(2):615–632, 1972.

[63] Kim D. O., C. E. Molnar, and R. R. Peiffer. A system of nonlinear differential equations modeling basilar-membrane motion. *Journal of the Acoustical Society of America*, 54:1517–1529, 1973.

[64] J.L. Hall. Two-tone distortion products in a nonlinear model of the basilar membrane. *Journal of the Acoustical Society of America*, 56:1818–1828, 1974.

[65] E. F. Evans and P. J. Wilson. Cochlear tuning properties: Concurrent basilar membrane and single nerve fiber measurement. *Science*, 190:1218–1221, December 1975.

[66] E. Zwicker and E. Terhardt. *Facts and models in hearing*. Springer-Verlag, Berlin, New York, 1974.

[67] J. B. Allen. Cochlear micromechanics - A mechanism for transforming mechanical to neural tuning within the cochlea. *Journal of the Acoustical Society of America*, 62:930–939, 1977.

[68] J.J. Zwislocki and E.J. Kletskey. Tectorial membrane: A possible effect on frequency analysis in the cochlea. *Science*, 204:639–641, 1979.

[69] Khanna S. M. and D. Leonard. Basilar membrane tuning in the cat cochlea. *Science*, 215:305–306, 1982.

[70] P.M. Sellick, R. Patuzzi, and B.M. Johnstone. Measurement of basilar membrane motion in the guinea pig using Mössbauer technique. *Journal of the Acoustical Society of America*, 72:131–140, 1982.

[71] S. M. Khanna and D. G. B. Leonard. Relationship between basilar membrane tuning and hair cell condition. *Hearing Research*, 23:55–70, 1986.

[72] P.M. Sellick, R. Patuzzi, and B.M. Johnstone. Comparison between the tuning properties of inner haircells and basilar membrane motion. *Hearing Research*, 10:93–100, 1983.

[73] P.M. Sellick, G.K. Yates, and R. Patuzzi. The influence of Mössbauer source size and position on phase and amplitude measurements of the guinea pig basilar membrane. *Hearing Research*, 10:101–108, 1983.

[74] D.T. Kemp. The evoked cochlear mechanical response and the auditory microstructure – evidence for a new element in cochlear mechanics. In *Models of the auditory system and related signal processing techniques*, 9, pages 35–47. Scandinavian Audiology, Supplementum 9, 1979.

[75] D.T. Kemp. Evidence of mechanical nonlinearity and frequency selective wave amplification in the cochlea. *Archives of Oto-Rhino-Laryngology*, 224:37–45, 1979.

[76] D.T. Kemp. Towards a model for the origin of cochlear echoes. *Hearing Research*, 2:533–548, 1980.

[77] D.T. Kemp. Otoacoustic emissions, travelling waves and cochlear mechanisms. *Journal of the Acoustical Society of America*, 22:95–104, 1986.

[78] J. B. Allen. OHCs shift the excitation pattern via BM tension. In E.R. Lewis, G.R. Long, R.F. Lyon, P.M. Narins, C.R. Steel, and E. Hecht-Poinar, editors, *Diversity in auditory mechanics*, pages 167–175. World Scientific Press, Singapore, 1997.

[79] David He and Peter Dallos. Somatic stiffness of cochlear outer hair cells is voltage-dependent. *Proceedings National Academy Science*, 96(14):8223–8228, July 1999.

[80] David He and Peter Dallos. Properties of voltage-dependent somatic stiffness of cochlear outer hair cells. *Journal of the Association for Research in Otolaryngology*, 1(1):64–81, July 2000.

[81] R.L. Wegel and C.E. Lane. The auditory masking of one pure tone by another and its probable relation to the dynamics of the inner ear. *Physical Review*, 23:266–285, February 1924.

[82] D.O. Kim, J.H. Siegel, and C.E. Molnar. Cochlear nonlinear phenomena in two-tone responses. In M. Hoke and E. DeBoer, editors, *Scandinavian Audiology, Supplementum 9*, pages 63–82, 1979.

[83] P. F. Fahey and J. B. Allen. Nonlinear phenomena as observed in the ear canal, and at the auditory nerve. *Journal of the Acoustical Society of America*, 77(2):599–612, February 1985.

[84] M. B. Sachs and Y. S. Kiang. Two-tone inhibition in auditory-nerve fibers. *Journal of the Acoustical Society of America*, 43:1120–1128, 1968.

[85] R.M. Arthur, R.R. Pfeiffer, and N. Suga. Properties of "two-tone inhibition" in primary auditory neurons. *J. Physiology (London)*, 212:593–609, 1971.

[86] P.J. Abbas and M.B. Sachs. Two–tone suppression in auditory–nerve fibers: Extension of a stimulus–response relationship. *Journal of the Acoustical Society of America*, 59(1):112–122, January 1976.

[87] X.D. Pang and J.J. Guinan. Growth rate of simultaneous masking in cat auditory-nerve fibers: Relationship to the growth of basilar-membrane motion and the origin of two-tone suppression. *Journal of the Acoustical Society of America*, 102(6):3564–3574, December 1997. Beautiful data showing the slope of suppression for low frequency suppressors.

[88] S.S. Narayan and M.A. Ruggero. Basilar-membrane mechanics at the hook region of the chinchilla cochlea. In *Mechanics of hearing, Zao*, Singapore, 2000. World Scientific.

[89] J. B. Allen. Response to deBoer regarding BM tuning. In H. Dufhuis, J. W. Horst, P. van Dijk, and S. M. van Netten, editors, *Biophysics of hair cell sensory systems*, page 304. World Scientific, Singapore, New Jersey, London, Hong Kong, 1993.

[90] J. B. Allen. Magnitude and phase-frequency response to single tones in the auditory nerve. *Journal of the Acoustical Society of America*, 73(6):2071–2092, 1983.

[91] J. B. Allen and P. F. Fahey. A second cochlear-frequency map that correlates distortion product, neural tuning measurements. *Journal of the Acoustical Society of America*, 94(2, Pt. 1):809–816, August 1993.

[92] S.S. Narayan, A.N. Temchin, A. Recio, and M.A. Ruggero. Frequency tuning of basilar membrane and auditory nerve fibers in the same cochleae. *Science*, 282:1882–1884, December 1998. Shows BM and neural differ by 3.8 dB/oct.

[93] E.P Fowler. A method for the early detection of otosclerosis. *Archives of otolaryngology*, 24(6):731–741, 1936.

[94] S.T. Neely and D. O. Kim. An active cochlear model showing sharp tuning and high sensitivity. *Hearing Research*, 9:123–130, 1983.

[95] A. M. Mayer. Research in acoustics. *Philosophy Magazine*, 2:500–507, 1876. In Benchmark Papers in Acoustics, vol. 13, Earl D. Schubert, Ed.

[96] E.B. Titchener. *Experimental Psychology, A Manual of Laboratory Practice, Vol. II*. The Macmillan Co., London, 1923.

[97] Jont B. Allen. Harvey Fletcher 1884–1981. In Jont B. Allen, editor, *The ASA edition of Speech, Hearing in Communication*, pages A1–A34. Acoustical Society of America, Woodbury, New York, 1995.

[98] Jont B. Allen. A short history of telephone psychophysics. *Audio Engineering Society*, Reprint 4636:1–37, September 1997.

[99] D McFadden. The curious half–octave shift: Evidence of a basalward migration of the traveling–wave envelope with increasing intensity. In R. Salvi, D. Henderson, R.P. Hamernik, and V. Coletti, editors, *Applied and Basic Aspects of Noise-Induced Hearing Loss*, pages 295–312. Plenum, 1986.

[100] W. A. Munson and M. B. Gardner. Loudness patterns–a new approach. *Journal of the Acoustical Society of America*, 22(2):177–190, March 1950.

[101] J. B. Allen. Psychoacoustics. In John G. Webster, editor, *Wiley Encyclopedia of Electrical and Electronics Engineering*, volume 17, pages 422–437. John Wiley & Sons, Inc, New York, NY, 1999.

[102] B. Delgutte. Two-tone suppression in auditory-nerve fibres: Dependence on suppressor frequency and level. *Hearing Research*, 49:225–246, 1990.

[103] B. Delgutte. Physiological mechanisms of psychophysical masking: Observations from auditory-nerve fibers. *Journal of the Acoustical Society of America*, 87:791–809, 1990.

[104] Bertrand Delgutte. Physiological models for basic auditory percepts. In H. Hawkins and T. McMullen, editors, *Auditory Computation*. Springer Verlag, New York, 1995.

[105] D.T. Kemp and R.A. Chum. Observations on the generator mechanism of stimulus frequency acoustic emissions–two tone suppression. In G. van den Brink and F.A. Bilsen, editors, *Psychological, Physiological and Behavioral Studies in Hearing*, pages 34–42, Delft, The Netherlands, 1980. Delft Univ. Press.

[106] E.J. Walsh and J. McGee. Frequency selectivity in the auditory periphery: Similarities between damaged and developing ears. *American Journal of Otolaryngology*, 11:23–32, 1990.

[107] L. Kanis and E. de Boer. Two-tone suppression in a locally active nonlinear model of the cochlea. *Journal of the Acoustical Society of America*, 96(4):2156–2165, October 1994.

[108] C. D. Geisler and A. L. Nuttall. Two-tone suppression of basilar membrane vibrations in the base of the guinea pig cochlea using “low-side” suppressors. *Journal of the Acoustical Society of America*, 102(1):430–440, jul 1997.

[109] E. deBoer. Mechanics of the cochlea: modeling efforts. In *The cochlea*, pages 258–317, New York, 1996. Springer.

[110] Daniel C. Geisler. *From Sound to Synapse: Physiology of the Mammalian Ear*. Oxford University Press, 1998.

[111] M.A. Ruggero, L. Robles, and N.C. Rich. Two-tone suppression in the basilar membrane of the cochlea: Mechanical basis of auditory-nerve rate suppression. *Journal of Neurophysiology*, 68(4):1087–1099, October 1992.

[112] N.P. Cooper. Two-tone suppression in cochlear mechanics. *Journal of the Acoustical Society of America*, 99(5):3087–3098, may 1996.

[113] Harvey Fletcher. The mechanism of hearing as revealed through experiments on the masking effect of thermal noise. *Proceedings National Academy Science*, 24:265–274, 1938.

[114] N.R. French and J.C. Steinberg. Factors governing the intelligibility of speech sounds. *Journal of the Acoustical Society of America*, 19:90–119, 1947.

[115] J.E. Hawkins and S.S. Stevens. The masking of pure tones and of speech by white noise. *Journal of the Acoustical Society of America*, 22(1):6–13, January 1950.

[116] A.R. Moller. Frequency selectivity of single auditory-nerve fibers in response to broadband noise stimuli. *Journal of the Acoustical Society of America*, 62(1):135–142, jul 1977.

[117] B.H. Deatherage, H. Davis, and D.H. Eldredge. Physiological evidence for the masking of low frequencies by high. *Journal of the Acoustical Society of America*, 29(1):132–137, January 1957. Early evidence of propagated distortion products. Remote masking.

[118] E. Zwicker and E. Schloth. Interrelation of different otoacoustic emissions. *Journal of the Acoustical Society of America*, 75:1148–1154, 1984.

[119] J. B. Allen, G. Shaw, and B. P. Kimberley. Characterization of the nonlinear ear canal impedance at low sound levels. *ARO*, 18(757):190, February 1995.

[120] E. Elliott. A ripple effect in the audiogram. *Nature*, 181:1076, 1958.

[121] P. M. Zurek. Spontaneous narrowband acoustic signals emitted by human ears. *Journal of the Acoustical Society of America*, 69:514–523, 1981.

[122] W. Bialek and H. P. Wit. Quantum limits to oscillator stability: Theory and experiments on acoustic emissions from the human ear. *Physics Letters*, 104a(3):173–178, 1984.

[123] Harvey Fletcher and J.C. Steinberg. The dependence of the loudness of a complex sound upon the energy in the various frequency regions of the sound. *Physical Review*, 24(3):306–317, September 1924.

[124] S. T. Neely and J. B. Allen. Relation between the rate of growth of loudness and the intensity DL. In W. Jesteadt and *et al.*, editors, *Modeling Sensorineural Hearing Loss*, pages 213–222. Lawrence Erlbaum, Inc., Hillsdale, NJ, 1996.

[125] William F. Carver. Loudness balance procedures. In Jack Katz, editor, *Handbook of Clinical Audiology, 2^d edition*, chapter 15, pages 164–178. Williams and Wilkins, Baltimore MD, 1978.

[126] Mark Gardner. Personal communication, 1994.

[127] J.C. Steinberg and M.B. Gardner. On the auditory significance of the term hearing loss. *Journal of the Acoustical Society of America*, 11:270–277, January 1940.

[128] Harvey Fletcher and W.A. Munson. Loudness, its definition, measurement, and calculation. *Journal of the Acoustical Society of America*, 5:82–108, 1933.

[129] Harvey Fletcher. A method of calculating hearing loss for speech from an audiogram. *Journal of the Acoustical Society of America*, 22:1–5, January 1950.

[130] J. B. Allen. Modeling the noise damaged cochlea. In P. Dallos, C. D. Geisler, J. W. Matthews, M. A. Ruggero, and C. R. Steele, editors, *The Mechanics and Biophysics of Hearing*, pages 324–332, New York, 1991. Springer-Verlag.

[131] Ning-ji He and Richard A. Schmiedt. Fine structure of the $2f_1 - f_2$ acoustic distortion product: changes with primary level. *Journal of the Acoustical Society of America*, 94(5):2659–2669, November 1993.

[132] S.T. Neely. Mathematical modeling of cochlear mechanics. *Journal of the Acoustical Society of America*, 78(1):345–352, 1985.

[133] S.T. Neely and D. O. Kim. A model for active elements in cochlear biomechanics. *Journal of the Acoustical Society of America*, 79:1472–1480, 1986.

[134] G. Zweig. Finding the impedance of the organ of Corti. *Journal of the Acoustical Society of America*, 89:1229–1254, 1991.

[135] J. B. Allen and P. F. Fahey. Using acoustic distortion products to measure the cochlear amplifier gain on the basilar membrane. *Journal of the Acoustical Society of America*, 92(1):178–188, July 1992.

[136] J. B. Allen. DeRecruitment by multiband compression in hearing aids. In B. Kollmeier, editor, *Psychoacoustics, speech, and hearing aids*, pages 141–152. World Scientific Press, Singapore, 1996.

[137] A. Papoulis. *Probability, Random Variables, and Stochastic Processes*. McGraw–Hill Book Co., New York, 1965.

[138] C.J. Kros and A.C. Crawford. Potassium currents in inner hair cells isolated from the guinea–pig cochlea. *Journal of Physiology*, 421:263–291, 1990.

[139] W. Denk and W.W. Webb. Forward and reverse transduction at the limit of sensitivity studied by correlating electrical and mechanical fluctions in frog saccular hair cells. *Hearing Research*, 60:89–102, 1992.

[140] I.J. Russell, Richardson, and Cody. Mechanosensitivity of mammalian auditory hair cells *in vitro*. *Nature*, 321(29):517–519, May 1986.

[141] J. J. Guinan and W. T. Peake. Middle-ear characteristics of anethetized cats. *Journal of the Acoustical Society of America*, 41:1237–1261, 1967.

[142] J.F. Ashmore. A fast motile response in guinea-pig outer hair cells: the molecular basis of the cochlear amplifier. *Journal of Physiology (London)*, 388:323–347, 1987.

[143] J. Santos-Sacchi. Reversible inhibition of voltage–dependent outer hair cell motility and capacitance. *J. of Neurosience*, 11(10):3096–3110, October 1991.

[144] K.H. Iwasa and R.S. Chadwick. Elasticity and active force generation of cochlear outer hair cells. *Journal of the Acoustical Society of America*, 92(6):3169–3173, December 1992.

[145] M Adachi, M. Sugawara, and K.H. Iwasa. Effect of turgor pressure on cell motility. *Journal of the Acoustical Society of America*, page Submitted, 2000.

[146] K.H. Iwasa. Effect of membrane motor on the axial stiffness of the cochlear outer hair cell. *Journal of the Acoustical Society of America*, 107:2764–2766, May 2000.

[147] Y. Fung. *Biomechanics*. Springer–Verlag, New York, NY, 1981.

[148] M Adachi and K.H. Iwasa. Electrically driven motor in the outer hair cell: Effect of a mechanical constraint. *Proceedings National Academy Science*, 96:7244–7249, jun 1999.

[149] Richard Feynman. *Feynman Lectures On Physics*. Addison-Wesley Pub. Co., 1970.

[150] C.R. Steele, G. Baker, J. Tolomeo, and D. Zetes. Electro-mechanical models of the outer hair cell. In H. Diufhuis, J. W. Horst, and H. P. Wit, editors, *Basic issues in hearing*, pages 207–214. Academic Press, London, 1993.

[151] K.H. Iwasa. Motor mechanisms of the outer hair cell from the cochlea. In Hiroshi Wada and Tomonori Takasaka, editors, *Recent Developments in Auditory Mechanics*. World Scientific Publishing Co., PO Box 128, Farrer Road, Singapore 912805, 1999.

[152] J.B. Allen. Derecruitment by multiband compression in hearing aids. In C.I. Berlin, editor, *The Efferent Auditory System*, chapter 4, pages 73–86. Singular, 401 West A St., Suite 325, San Diego, CA 92101, 1999. Includes a CDROM video talk by Jont Allen in MP3 format.

[153] J.B. Allen and Deep Sen. Is tectorial membrane filtering required to explain two tone suppression and the upward spread of masking? In Hiroshi Wada, Tomonori Takasaka, K. Kieda, K. Ohyama, and T. Koike, editors, *Recent Developments in Auditory Mechanics*, chapter The cochlea (measurement), pages 137–143. World Scientific Publishing Co., PO Box 128, Farrer Road, Singapore 912805, 1999.

[154] J. B. Allen and P. F. Fahey. Nonlinear behavior at threshold determined in the auditory canal on the auditory nerve. In R. Klinke and R. Hartman, editors, *Hearing – Physiological bases and psychophysics*, pages 128–134. Springer-Verlag, Bad Nauheim, Germany, 1983.

[155] J. B. Allen and B. L. Lonsbury-Martin. Otoacoustic emissions. *Journal of the Acoustical Society of America*, 93(1):568–569, January 1993.

[156] P. F. Fahey and J. B. Allen. Measurement of distortion product phase in the ear canal of cat. *Journal of the Acoustical Society of America*, 102(5):2880–2891, November 1997.

[157] S.T. Neely. A model of cochlear mechanics with outer hair cell motility. *Journal of the Acoustical Society of America*, 1992.

[158] R.J. Diependaal, E. de Boer, and M.A. Viergever. Cochlear power flux as an indicator of mechanical activity. *Journal of the Acoustical Society of America*, 82:917–926, 1987.

[159] E deBoer and A.L. Nuttall. The “inverse problem” solved for a three-dimensional model of the cochlear. III brushing-up the solution method. *Journal of the Acoustical Society of America*, 105(6):3410–3420, 1999. need exact reference.

[160] E deBoer and A.L. Nuttall. The mechanical waveform of the basilar membrane. II. from data to models–and back. *Journal of the Acoustical Society of America*, 107(3):1487–1496, 2000.

[161] E deBoer and A.L. Nuttall. The mechanical waveform of the basilar membrane. III. intensity effects. *Journal of the Acoustical Society of America*, 107(3):1496–1507, 2000.

[162] D.O. Kim, S.T. Neely, C.E. Molnar, and J.W. Matthews. An active cochlear model with negative damping in the cochlear partition: Comparison with rhode’s ante- and post-mortem results. In G. van den Brink and F.A. Bilsen, editors, *Psychological, Physiological and Behavioral Studies in Hearing*, pages 7–14, Delft, The Netherlands, 1980. Delft Univ. Press.

[163] D.C. Mountain, A.E. Hubbard, and T.A. McMullen. Electromechanical processes in the cochlea. In E. de Boer and M.A. Viergever, editors, *Mechanics of Hearing*, pages 119–126, Netherlands, 1983. Delft Univ.

[164] P. Dallos, C.D. Geisler, J.W. Matthews, M.A. Ruggero, and C.R. Steele. *The Mechanics and Biophysics of Hearing*. Springer-Verlag, New York, 1991.